the subjective functional parameters, such as the ALSFRS-R and modified Norris score, indicating that motor functional deficits at an early stage of the disease may not be detected using these measures. By contrast, the estimated values at onset were far more or less than the normal level for the objective outcome measures, such as the 6-min walk distance, grip power and serum creatine kinase and creatinine levels, implying that disease severity may be evaluated by using these objective measures. Thus, our findings suggest that the objective and quantitative assessments, but not functional scales, are sensitive measures to detect subtle clinical deficits at an early or preclinical stage of spinal and bulbar muscular atrophy.

Clinical phenotypes and onset site distribution of spinal and bulbar muscular atrophy

In the analyses of the baseline data, we noticed that the degree of bulbar symptoms do not necessary correspond to that of limb involvement. For instance, pharyngeal barium residue, a clinical measure of dysphagia, was relatively little in certain patients who showed a decreased 6-min walk distance (Patients 9 and 11; Supplementary Table 10). Conversely, walking capacity was relatively preserved in Patients 28 and 32 who demonstrated increased barium residue in videofluorography. These findings prompted us to categorize the clinical symptoms of spinal and bulbar muscular atrophy with respect to the site of involvement using factor analysis (Fig. 3 and Supplementary material). This result suggests that upper limb function is closely related to bulbar function, but not to lower limb function. To confirm this view, the relationship among each domain of ALSFRS-R and that of the modified Norris score were investigated. The results showed that upper limb function is closely related to bulbar function compared with lower limb function, supporting the findings of our factor analysis (Supplementary Table 11). These observations suggest that the phenotypes of spinal and bulbar muscular atrophy may take a bulbar/upper limb-dominant or lower limb-dominant form. However, subgroup analyses according to the initially affected site showed no substantial differences between the patients whose initial symptom were bulbar or upper limb weakness and those who first noticed lower limb symptoms (Supplementary Table 12).

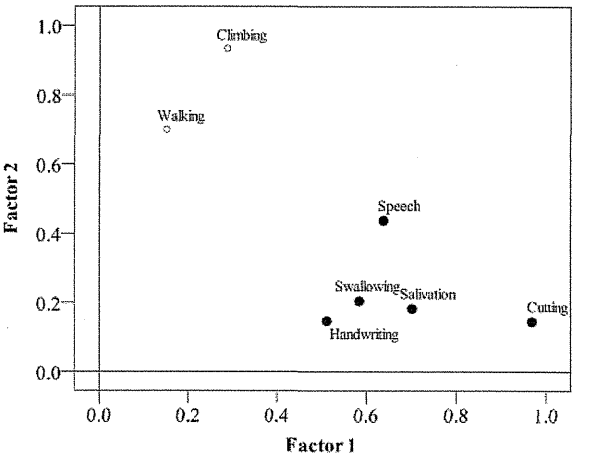

Figure 3 Factor analysis of ALSFRS-R subscores. Plot of variables for Factors 1 and 2 derived from factor analyses. Each variable indicates the items of the ALSFRS-R.
Climbing = climbing stairs; Cutting = cutting food and handling utensils.

Discussion

Spinal and bulbar muscular atrophy is a relatively rare neurodegenerative disease, for which the data regarding longitudinal analyses of clinical measures are limited (Katsuno *et al.* 2010; Fernández-Rhodes *et al.* 2011). The 3-year natural history data of quantitative outcome measures in spinal and bulbar muscular atrophy obtained from the present study will be useful for the design of future therapeutic trials, including the choice of outcome measures, determination of the observation period, stratification of patients and calculation of the sample size. In our longitudinal analyses, all of the outcome measures, except for the ALSAQ-5 and barium residue, showed a statistically significant progression, suggesting a slow but steady deterioration of symptoms in patients with spinal and bulbar muscular atrophy. The lack of significant longitudinal changes of pharyngeal barium residue may result from unequivocal variation among patients and piecemeal deglutition, a possible compensatory mechanism against slowly progressive bulbar palsy, which may hinder the measurement of the residue in patients with spinal and bulbar muscular atrophy (Katsuno *et al.*, 2010).

The results of sample size calculation indicated that the employment of functional rating scales as the primary endpoint may reduce the sample size. However, even with these functional outcome measures, clinical trials of disease-modifying therapies that suppress the exacerbation of symptoms appear to be less practical than those testing symptomatic therapies. Furthermore, these scales are shown to be more susceptible to placebo effects than objective measures (Hashizume *et al.*, 2012). This issue should also be taken into account to design clinical trials of spinal and bulbar muscular atrophy using subjective outcome measures. In addition, the effect of ageing on outcome measures is an alternative factor that may compromise the sample size estimation. Since motor function declines with age, the longitudinal changes of outcome measures in the present study might contain both disease-specific and age-related deterioration of function. This issue appears to be particularly critical when using objective measures, whereas the effects of ageing appear to be less problematic for subjective measures, the score of which is expected to be full even in aged subjects with normal activity. For instance, previous studies suggest that the 6-min walk distance test shows an age-dependent decline at ~5 m/year that may lead to the overestimation of disease progression in patients with spinal and bulbar muscular atrophy (Enright *et al.*, 1998; Takeuchi *et al.*, 2008).

In this longitudinal study, we also analysed the individual raw data in consideration of disease duration because it influences the severity of the neurological symptoms of spinal and bulbar muscular atrophy (Takeuchi *et al.*, 2008; Rhodes *et al.*, 2009). To this end, we summarized the individual data into a representative line by using random coefficient regression models. The results indicated that the disease progression is relatively linear, rather than quadratic or exponential, in the population studied (Fig. 2). The slope of the line was equivalent to the actual disease progression calculated for each parameter, indicating the plausibility of this modelling process (Table 3). This result raised the possibility that the data from the present study can be used as comparative historical control data in future clinical studies.

In the present study, we also confirmed that CAG repeat length correlated well with the age of onset and other activity of daily living milestones, as previously shown in spinal and bulbar muscular atrophy and other polyglutamine diseases (Abe *et al.*, 1998; Stevanin *et al.*, 2000; Atsuta *et al.*, 2006; Walker, 2007; Reetz *et al.*, 2011). In contrast to the strong correlation of CAG repeat size with the age at onset, the disease progression of spinal and bulbar muscular atrophy was not affected by CAG repeat length in androgen receptor. This result may suggest that the size of the CAG repeat influences the timing of the onset of clinical symptoms, but not the progression of neurological deficits, and that different mechanisms underlie disease initiation and progression in spinal and bulbar muscular atrophy (Atsuta *et al.*, 2006). In support of this view, the onset of motor dysfunction is reportedly determined by the expression of causative proteins in neurons, but disease progression is largely dependent on glial pathology, in a mutant super oxide dismutase 1 mouse model of amyotrophic lateral sclerosis (Boille *et al.*, 2006). Alternatively, the length of the CAG repeat may determine the nucleation speed of pathogenic androgen receptor proteins and the eventual onset of disease, but not the rate of aggregation that is likely to influence progression (Zhou *et al.*, 2011). It can also be inferred that the older age at onset in patients with a shorter CAG repeat may lead to accelerated progression, which overwhelms the direct effects of genotype on the post-onset course of the disease. This may underlie the faster deterioration of timed walking and serum creatinine levels in the patients with a shorter CAG repeat (Supplementary Table 6). In our subgroup analyses considering age at onset, patients with an older age of onset tended to show a more rapid deterioration of timed walking and serum creatinine levels, although the intergroup differences were not significant (Supplementary Table 7).

Laboratory tests often detect high serum levels of creatine kinase in patients with spinal and bulbar muscular atrophy, a possible clue to early diagnosis (Sorarù *et al.*, 2008; Chahin and Sorenson, 2009; Rhodes *et al.*, 2009). Our results of the baseline analysis suggested that the elevation of creatine kinase and the decrease of creatinine levels in serum were the most characteristic blood findings in patients with spinal and bulbar muscular atrophy. Since there are no established blood markers for spinal and bulbar muscular atrophy, it is important to determine if each blood index can be used as a biomarker to evaluate the effects of tested therapies in future clinical trials. In the present study, multiple regression analyses using baseline data raised the possibility that the serum level of creatinine is a reliable biomarker of disease severity. Creatinine is a biosysthetic product of creatine phosphate, which is a key molecule for energy production in muscle. Creatine is converted to creatinine and transported from muscle through the circulation to the kidneys (Viollet *et al.*, 2009). Because the serum creatinine level is associated with the whole muscle mass, it may be a useful marker for monitoring disease progression in spinal and bulbar muscular atrophy. The correlation between the serum levels of creatinine and clinical severity also suggested that the precise measurement of the whole muscle mass is essential to develop new biomarkers. Conversely, the serum level of creatine kinase was not correlated with most of the outcome measures, possibly because it is vulnerable to the patient's activity before blood sampling. Therefore, careful management of the patient's activity before sampling appears to be necessary when the serum levels of creatine kinase are used as a biomarker of spinal and bulbar muscular atrophy (Banno *et al.*, 2009).

Preventive or early intervention is construed as a key factor for successful translational research on disease-modifying therapies for neurodegenerative diseases (Holtzman, 2008). With regard to spinal and bulbar muscular atrophy, the results of phase III trials suggest that leuprorelin might be more effective in patients whose disease duration is <10 years (Katsuno *et al.*, 2010). These observations imply the need to evaluate disease severity at an early stage using sensitive clinical markers to facilitate clinical trials of disease-modifying therapies. In the longitudinal analyses of the present study, it was suggested that the biological or neurological deficit at a preclinical or early stage of the disease might be detectable using objective functional or blood parameters, but not using subjective outcome measures. In support of these findings, the reduction of brain volume and the decline of quantitative motor function were demonstrated in pre-manifest carriers in a prospective analysis of the natural history of Huntington's disease (Tabrizi *et al.*, 2009). These results might suggest the need to adopt appropriate objective measures for designing clinical trials of early interventions, and to reconsider the conventional definition of the onset of neurodegenerative diseases, including spinal and bulbar muscular atrophy, on the basis of the patients' perception of subjective symptoms for the development of disease-modifying therapies. The variability of onset age with a similar CAG repeat length may also suggest the limit of clinical definition of disease onset (Supplementary Table 9).

On the basis of the observation that the degree of bulbar involvement is not necessarily similar to that of limb impairment, we analysed the clinical phenotype of spinal and bulbar muscular atrophy using baseline data. The results indicated that upper limb function is closely related to bulbar function, but not to lower limb function and that patients with spinal and bulbar muscular atrophy appear to be diverse in terms of the preferentially affected site. These observations suggest that the severity of neurodegeneration may be associated with neuroanatomical closeness in spinal and bulbar muscular atrophy. In support of this view, the degeneration of neurons is shown to affect the dynamics of cell death in neighbouring cells (Friedlander, 2003). Additionally, disease-specific patterns of the topographical expansion of pathology have been suggested for several neurodegenerative diseases (Goedert *et al.*, 2010).

In summary, the results of the present study demonstrated the slow but steady progression of motor impairment in spinal and bulbar muscular atrophy. Analyses using random coefficient models did not indicate that the disease progression of spinal and bulbar muscular atrophy is substantially affected by the CAG repeat length, the age of onset, or serum levels of testosterone, suggesting that these variables may not be critical factors for the stratification of patients in clinical trials. Biological and neurological deficits were detectable using objective functional or blood parameters, even during the early or preclinical stage of spinal and bulbar muscular atrophy, suggesting that these indices may be used as endpoints in clinical trials of disease-modifying therapies for spinal and bulbar muscular atrophy.

Funding

This work was supported by a Center-of-Excellence (COE) grant, a Grant-in-Aid for Scientific Research on Innovated Areas 'Foundation of Synapse and Neurocircuit Pathology' and Grants-in-Aid from the Ministry of Education, Culture, Sports, Science and Technology of Japan; grants from the Ministry of Health, Labor, and Welfare of Japan; and Core Research for Evolutional Science and Technology (CREST) from the Japan Science and Technology Agency (JST). There were no other funding sources, and the investigators had sole discretion over study design, collection, analysis and interpretation of data, writing of the report and decision to submit it for publication.

Supplementary material

Supplementary material is available at *Brain* online.

References

Abe Y, Tanaka F, Matsumoto M, Doyu M, Hirayama M, Kachi T, et al. CAG repeat number correlates with the rate of brainstem and cerebellar atrophy in Machado-Joseph disease. Neurology 1998; 51: 882–4.

Akaike H. Information theory and an extension of the maximum likelihood principle. In: Petrov BC, editor. Proceedings of the Second International Symposium on Information Theory. Budapest, Hungary: Akademia Kiado; 1973. p. 267–81.

Atsuta N, Watanabe H, Ito M, Banno H, Suzuki K, Katsuno M, et al. Natural history of spinal and bulbar muscular atrophy (SBMA): a study of 223 Japanese patients. Brain 2006; 129: 1446–55.

Banno H, Adachi H, Katsuno M, Suzuki K, Atsuta N, Watanabe H, et al. Mutant androgen receptor accumulation in spinal and bulbar muscular atrophy scrotal skin: a pathogenic marker. Ann Neurol 2006; 59: 520–6.

Banno H, Katsuno M, Suzuki K, Takeuchi Y, Kawashima M, Suga N, et al. Phase 2 trial of leuprorelin in patients with spinal and bulbar muscular atrophy. Ann Neurol 2009; 65: 140–50.

Barkhaus PE, Kennedy WR, Stern LZ, Harrington RB. Hereditary proximal spinal and bulbar motor neuron disease of late onset. A report of six cases. Arch Neurol 1982; 39: 112–6.

Besinger UA, Toyka KV, Hömberg M, Heininger K, Hohlfeld R, Fateh-Moghadam A. Myasthenia gravis: long-term correlation of binding and bungarotoxin blocking antibodies against acetylcholine receptors with changes in disease severity. Neurology 1983; 33: 1316–21.

Boillée S, Yamanaka K, Lobsiger CS, Copeland NG, Jenkins NA, Kassiotis G, et al. Onset and Progression in Inherited ALS Determined by Motor Neurons and Microglia. Science 2006; 312: 1389–92.

Chahin N, Sorenson EJ. Serum creatine kinase levels in spinobulbar muscular atrophy and amyotrophic lateral sclerosis. Muscle Nerve 2009; 40: 126–9.

Chevalier-Larsen ES, O'Brien CJ, Wang H, Jenkins SC, Holder L, Lieberman AP, et al. Castration restores function and neurofilament alterations of aged symptomatic males in a transgenic mouse model of spinal and bulbar muscular atrophy. J Neurosci 2004; 24: 4778–86.

Dejager S, Bry-Gauillard H, Bruckert E, Eymard B, Salachas F, LeGuern E, et al. A comprehensive endocrine description of Kennedy's disease revealing androgen insensitivity linked to CAG repeat length. J Clin Endocrinol Metab 2002; 87: 3893–901.

Deschaintre Y, Richard F, Leys D, Pasquier F. Treatment of vascular risk factors is associated with slower decline in Alzheimer disease. Neurology 2009; 73: 674–80.

Doyu M, Sobue G, Mukai E, Kachi T, Yasuda T, Mitsuma T, et al. Severity of X-linked recessive bulbospinal neuronopathy correlates with size of the tandem CAG repeat in androgen receptor gene. Ann Neurol 1992; 32: 707–10.

Enright PL, Sherrill DL. Reference equations for the six-minute walk in healthy adults. Am J Respir Crit Care Med 1998; 158: 1384–7.

Fernández-Rhodes LE, Kokkinis AD, White MJ, Watts CA, Auh S, Jeffries NO, et al. Efficacy and safety of dutasteride in patients with spinal and bulbar muscular atrophy: a randomised placebo-controlled trial. Lancet Neurol 2011; 10: 140–7.

Fischbeck KH. Kennedy disease. J Inherit Metab Dis 1997; 20: 152–8.

Friedlander RM. Apoptosis and caspases in neurodegenerative diseases. N Engl J Med 2003; 348: 1365–75.

Goedert M, Clavaguera F, Tolnay M. The propagation of prion-like protein inclusions in neurodegenerative diseases. Trends Neurosci 2010; 33: 317–25.

Hashizume A, Katsuno M, Banno H, Suzuki K, Suga N, Tanaka F, et al. Differential change of clinical outcome measures in spinal and bulbar muscular atrophy. -Comparison of natural history with placebo-treated group-. J Neurol 2012; 259: 712–9.

Holtzman DM. Alzheimer's disease: moving towards a vaccine. Nature 2008; 454: 418–20.

James R. Brinkmann, Patricia Andres, Michelle Mendoza, Mohammed Sanjak. Guidelines for the use and performance of quantitative outcome measures in ALS clinical trials. J Neurol Sci 1997; 147: 97–111.

Jenkinson C, Fitzpatrick R, Brennan C, Bromberg M, Swash M. Development and validation of a short measure of health status for individuals with amyotrophic lateral sclerosis/motor neurone disease: the ALSAQ-40. J Neurol 1999; 246(Suppl 3): III16–21.

Jenkinson C, Fitzpatrick R. Reduced item set for the amyotrophic lateral sclerosis assessment questionnaire: development and validation of the ALSAQ-5. J Neurol Neurosurg Psychiatry 2001; 70: 70–3.

Katsuno M, Adachi H, Kume A, Li M, Nakagomi Y, Niwa H, et al. Testosterone reduction prevents phenotypic expression in a transgenic mouse model of spinal and bulbar muscular atrophy. Neuron 2002; 35: 843–54.

Katsuno M, Adachi H, Doyu M, Minamiyama M, Sang L, Kobayashi Y, et al. Leuprorelin rescues polyglutamine-dependent phenotypes in a transgenic mouse model of spinal and bulbar muscular atrophy. Nat Med 2003; 9: 768–73.

Katsuno M, Banno H, Suzuki K, Takeuchi Y, Kawashima M, Yabe I, et al. Efficacy and safety of leuprorelin in patients with spinal and bulbar muscular atrophy (JASMITT study): a multicentre, randomised, double-blind, placebo-controlled trial. Lancet Neurol 2010; 9: 875–84.

Katsuno M, Banno H, Suzuki K, Adachi H, Tanaka F, Sobue G. Molecular pathophysiology and disease-modifying therapies for spinal and bulbar muscular atrophy. Arch Neurol 2012; 69: 436–40.

Kennedy WR, Alter M, Sung JH. Progressive proximal spinal and bulbar muscular atrophy of late onset. A sex-linked recessive trait. Neurology 1968; 18: 671–80.

Kuhlemeier KV, Yates P, Palmer JB. Intra- and inter-rater variation in the evaluation of videofluorographic swallowing studies. Dysphagia 1998; 13: 142–7.

Laird NM, Ware JH. Random-effects models for longitudinal data. Biometrics 1982; 38: 963–74.

La Spada AR, Wilson EM, Lubahn DB, Harding AE, Fischbeck KH. Androgen receptor gene mutations in X-linked spinal and bulbar muscular atrophy. Nature 1991; 352: 77–9.

La Spada AR, Taylor JP. Polyglutamines placed into context. Neuron 2003; 38: 681–4.

Logemann JA, Kahrilas PJ, Kobara M, Vakil NB. The benefi t of head rotation on pharyngoesophageal dysphagia. Arch Phys Med Rehabil 1989; 70: 767–71.

Logemann JA, Pauloski BR, Rademaker AW, Colangelo LA, Kahrilas PJ, Smith CH. Temporal and biomechanical characteristics of oropharyngeal swallow in younger and older men. J Speech Lang Hear Res 2000; 43: 1264–74.

McLean RA, Sanders WL, Stroup WW. A unified approach to mixed linear models. Am Stat 1991; 45: 54–64.

Montes J, McDermott MP, Martens WB, Dunaway S, Glanzman AM, Riley S, et al. Six-Minute Walk Test demonstrates motor fatigue in spinal muscular atrophy. Neurology 2010; 74: 833–8.

Nandhagopal R, Kuramoto L, Schulzer M, Mak E, Cragg J, Lee CS, et al. Longitudinal progression of sporadic Parkinson's disease: a multi-tracer positron emission tomography study. Brain 2009; 2970–9.

Oda E, Ohashi Y, Tashiro K, Mizuno Y, Kowa H, Yanagisawa N. Reliability and factorial structure of a rating scale for amyotrophic lateral sclerosis. No To Shinkei 1996; 48: 999–1007.

Ohashi Y, Tashiro K, Itoyama Y, Nakano I, Sobue G, Nakamura S, et al. Study of functional rating scale for amyotrophic lateral sclerosis: revised ALSFRS (ALSFRS-R) Japanese version. No To Shinkei 2001; 53: 346–55.

Orr HT, Zoghbi HY. Trinucleotide repeat disorders. Annu Rev Neurosci 2007; 30: 575–621.

Rascol O. 'Disease-modification' trials in Parkinson disease: target populations, endpoints and study design. Neurology 2009; 72: 51–8.

Reetz K, Kleinman A, Klein C, Lencer R, Zuehlke C, Brockmann K, et al. CAG repeats determine brain atrophy in spinocerebellar ataxia 17: VBM study. PLoS One 2011; 19: e15125.

Rhodes LE, Freeman BK, Auh S, Kokkinis AD, La Pean A, Chen C, et al. Clinical features of spinal and bulbar muscular atrophy. Brain 2009; 132: 3242–51.

Schmidt BJ, Greenberg CR, Allingham-Hawkins DJ, Spriggs EL. Expression of X-linked bulbospinal muscular atrophy (Kennedy disease) in two homozygous women. Neurology 2002; 59: 770–2.

Searle SR. Mixed models and unbalanced data: wherefrom, whereat, and whereto? Commun Stat Theory Methods 1988; 17: 935–68.

Sinnreich M, Sorenson EJ, Klein CJ. Neurologic course, endocrine dysfunction and triplet repeat size in spinal bulbar muscular atrophy. Can J Neurol Sci 2004; 31: 378–82.

Sobue G, Hashizume Y, Mukai E, Hirayama M, Mitsuma T, Takahashi A. X-linked recessive bulbospinal neuronopathy. A clinicopathological study. Brain 1989; 112: 209–32.

Sorarù G, D'Ascenzo C, Polo A, Palmieri A, Baggio L, Vergani L, et al. Spinal and bulbar muscular atrophy: skeletal muscle pathology in male patients and heterozygous females. J Neurol Sci 2008; 264: 100–5.

Sperfeld AD, Karitzky J, Brummer D, Schreiber H, Häussler J, Ludolph AC, et al. X-linked bulbospinal neuronopathy: Kennedy disease. Arch Neurol 2002; 59: 1921–6.

Stevanin G, Dürr A, Brice A. Clinical and molecular advances in autosomal dominant cerebellar ataxias: from genotype to phenotype and physiology. Eur J Hum Gen 2000; 8: 4–18.

Tabrizi SJ, Langbehn DR, Leavitt BR, Roos RA, Durr A, Craufurd D, et al. Biological and clinical manifestations of Huntington's disease in the longitudinal TRACK-HD study: cross-sectional analysis of baseline data. Lancet Neurol 2009; 8: 791–801.

Takeuchi Y, Katsuno M, Banno H, Suzuki K, Kawashima M, Atsuta N, et al. Walking capacity evaluated by the 6-minute walk test in spinal and bulbar muscular atrophy. Muscle Nerve 2008; 38: 964–71.

The ALS CNTF treatment study (ACTS) phase I-II Study Group. The Amyotrophic Lateral Sclerosis Functional Rating Scale. Assessment of activities of daily living in patients with amyotrophic lateral sclerosis. Arch Neurol 1996; 53: 141–7.

Viollet L, Gailey S, Thornton DJ, Friedman NR, Flanigan KM, Mahan JD, et al. Utility of cystatin C to monitor renal function in Duchenne muscular dystrophy. Muscle Nerve 2009; 40: 438–42.

Walker FO. Huntington's disease. Lancet 2007; 369: 218–28.

Williams DR, de Silva R, Paviour DC, Pittman A, Watt HC, Kilford L, et al. Characteristics of two distinct clinical phenotypes in pathologically proven progressive supranuclear palsy: Richardson's syndrome and PSP-parkinsonism. Brain 2005; 128: 1247–58.

Yamaguchi T, Ohbu S, Saito M, Ito Y, Morikawa F, Tashiro K, et al. Validity and clinical applicability of the Japanese version of amyotrophic lateral sclerosis assessment questionnaire 40 (ALSAQ-40). No To Shinkei 2004; 56: 483–94.

Zhou ZL, Zhao JH, Liu HL, Wu JW, Liu KT, Chuang CK, et al. The possible structural models for polyglutamine aggregation: a molecular dynamics simulations study. J Biomol Struct Dyn 2011; 28: 743–58.

Neurobiology of Disease 45 (2012) 862–870

Contents lists available at SciVerse ScienceDirect

Neurobiology of Disease

journal homepage: www.elsevier.com/locate/ynbdi

Oxidative stress induced by glutathione depletion reproduces pathological modifications of TDP-43 linked to TDP-43 proteinopathies

Yohei Iguchi [a], Masahisa Katsuno [a], Shinnosuke Takagi [a], Shinsuke Ishigaki [a,d], Jun-ichi Niwa [b], Masato Hasegawa [c], Fumiaki Tanaka [a], Gen Sobue [a,d,*]

[a] Department of Neurology, Nagoya University Graduate School of Medicine, 65 Tsurumai-cho, Showa-ku, Nagoya 466–8550, Japan
[b] Stroke Center, Aichi Medical University, Aichi 480–1195, Japan
[c] Departments of Molecular Neurobiology, Tokyo Institute of Psychiatry, Tokyo Metropolitan Organization for Medical Research, 2-1-8 Kamikitazawa, Setagaya-ku, Tokyo 156–8585, Japan
[d] CREST, Japan Science and Technology Agency, 4-1-8, Honcho, Kawaguchi, Saitama 332–0012, Japan

ARTICLE INFO

Article history:
Received 30 March 2011
Revised 29 August 2011
Accepted 4 December 2011
Available online 13 December 2011

Keywords:
TAR DNA-binding protein 43 kDa (TDP-43)
TDP-43 proteinopathy
Oxidative stress
Glutathione depletion
Post-translational modification
Protein phosphorylation

ABSTRACT

TAR DNA-binding protein 43 (TDP-43) is a major component of ubiquitin-positive inclusion of TDP-43 proteinopathies including amyotrophic lateral sclerosis and frontotemporal lobar degeneration with ubiquitinated inclusions, which is now referred to as FTLD-TDP. TDP-43 in the aberrant inclusion is known to be hyperphosphorylated at C-terminal sites, to be truncated at the N-terminal region, and to re-distribute from nucleus to cytoplasm or neurite. The pathogenic role of these modifications, however, has not been clarified. Furthermore, there is no evidence about the initial cause of these modifications. Herein we show that ethacrynic acid (EA), which is able to increase cellular oxidative stress through glutathione depletion, induces TDP-43 C-terminal phosphorylation at serine 403/404 and 409/410, insolubilization, C-terminal fragmentation, and cytoplasmic distribution in NSC34 cells and primary cortical neurons. In the investigation using a nonphosphorylable mutant of TDP-43, there was no evidence that C-terminal phosphorylation of TDP-43 contributes to its solubility or distribution under EA induction. Our findings suggest that oxidative stress induced by glutathione depletion is associated with the process of the pathological TDP-43 modifications and provide new insight for TDP-43 proteinopathies.

Introduction

TAR DNA-binding protein 43 (TDP-43) is a major component of ubiquitin-positive inclusion, a pathological hallmark of TDP-43 proteinopathies including amyotrophic lateral sclerosis (ALS) and frontotemporal lobar degeneration with ubiquitinated inclusions, which is now referred to as FTLD-TDP (Arai et al., 2006; Neumann et al., 2006). Both diseases occur in sporadic or familial forms, and are characterized by late-onset progressive deterioration of motor and/or cognitive function. TDP-43 is a heterogeneous nuclear ribonucleoprotein (hnRNP), which is known to regulate gene transcription and exon splicing through interactions with RNA, hnRNPs, and nuclear bodies (Ayala et al., 2005; Buratti et al., 2005; Wang et al., 2002, 2004). In addition, this protein has also been reported to stabilize human low molecular weight neurofilament (hNFL) mRNA through direct interaction with its 3'UTR (Strong et al., 2007), regulate retinoblastoma protein phosphorylation through the repression of cyclin-dependent kinase 6 (Cdk6) expression (Ayala et al., 2008), regulate activity of Rho family GTPases (Iguchi et al., 2009), and alter the expression of selected microRNAs, such as let-7b and miR-663 (Buratti et al., 2010). Furthermore, very recent works using cross-linking immunoprecipitation sequencing show that multiple RNAs interact with TDP-43 (Polymenidou et al., 2011; Sephton et al., 2011; Tollervey et al., 2011).

Although it mostly localizes in the nucleus under normal conditions, TDP-43 is distributed from nucleus to cytoplasm or neurite, and forms aggregates consisting mainly of C-terminal fragments in affected neurons of patients with TDP-43 proteinopathies. In addition, TDP-43 in the aberrant aggregation is hyperphosphorylated at multiple C-terminal sites (Hasegawa et al., 2008). However, neither the pathogenic role nor the initial cause of these abnormal modifications of TDP-43 has been elucidated. The fact that the majority of patients with TDP-43 proteinopathies are sporadic suggests that exogenous factors induce post-translational modifications of TDP-43 that are seen in the disease. Furthermore, TDP-43 inclusions have also been observed in Alzheimer disease (AD), Parkinson disease (PD),

Abbreviations: TDP-43, TAR DNA-binding protein of 43 kDa; ALS, amyotrophic lateral sclerosis; hnRNP, heterogeneous nuclear ribonucleoprotein; hNFL, human low molecular weight neurofilament; Cdk6, cyclin-dependent kinase 6; ROS, reactive oxygen species; EA, ethacrynic acid; NAC, N-acetylcysteine; CK1, casein kinase 1; CK2, casein kinase 2; WT-TDP-43, wild type TDP-43; SA-TDP-43, nonphosphorylable TDP-43.

* Corresponding author at: Department of Neurology, Nagoya University Graduate School of Medicine, 65 Tsurumai-cho, Showa-ku, Nagoya 466–8550, Japan. Fax: +81 52 744 2785.
E-mail address: sobueg@med.nagoya-u.ac.jp (G. Sobue).

Available online on ScienceDirect (www.sciencedirect.com).

0969-9961/$ – see front matter © 2011 Elsevier Inc. All rights reserved.
doi:10.1016/j.nbd.2011.12.002

dementia with Lewy bodies (DLB), and Huntington disease (HD), argyrophilic grain disease, suggesting that the aggregation of this protein may be a secondary feature of neurodegeneration (Amador-Ortiz et al., 2007; Arai et al., 2009, 2010; Geser et al., 2008; Hasegawa et al., 2007). These findings complicate understanding of the pathogenic role of TDP-43. On the other hand, there is considerable evidence that reactive oxygen species (ROS) and oxidative stress are associated with many neurodegenerative conditions including ALS (Abe et al., 1995, 1997; Beal et al., 1997; Butterfield et al., 2007; Ferrante et al., 1997; Lovell and Markesbery, 2007; Nunomura et al., 2002; Shaw et al., 1995). Herein we show that oxidative stress induced by glutathione depletion reproduces the pathological modifications of TDP-43, that are seen in TDP-43 proteinopathies, in motor neuron-like cells and primary cortical neurons.

Materials and methods

Cell culture and treatment

Mouse NSC34 motor neuron-like cells (a kind gift of N.R. Cashman, University of British Columbia, Vancouver, Canada) were cultured in a humidified atmosphere of 95% air-5% CO2 in a 37 °C incubator in Dulbecco's Modified Eagle's Medium (DMEM) supplemented with 10% fetal bovine serum (FBS). To differentiate the cells, the medium was changed to DMEM containing 1% FBS and 1% NEAA, and was cultured for 24 h. For the interventions, the cells were then incubated with ethacrynic acid (EA) (Sigma-Aldrich, St. Louis, MO), with or without N-acetylcysteine (NAC) (Sigma-Aldrich), casein kinase 1 (CK1) inhibitor (D4476), or casein kinase 2 (CK2) inhibitor (TBCA) (Sigma-Aldrich). Primary cultures of mouse embryonic cortical neurons that were dissociated from embryonic cortex of embryonic day 15 (E15) C57BL/6 J pregnant mice were plated onto poly-L-lysine-coated plates or glass bottom dishes, and maintained in neuron culture medium (Sumilon, Osaka, Japan). Five days after the incubation, the indicated interventions were performed. In both NSC34 cells and primary cortical neurons, the transfections of the intended plasmids were performed using Lipofectamine 2000 (Invitrogen, Eugene, OR), according to the manufacturer's instructions.

DNA constructs

Human wild type TDP-43 (WT-TDP-43) (accession number NM 007375) cDNA was amplified by PCR from cDNA of human spinal cord using the following primers: 5′-CACCATGTCTGAATATATTCGGGTAAC-3′ and 5′-CTACATTCCCCAGCCAGAAGACTTAGAAT-3′. The PCR product was cloned into the pENTR/D-TOPO vector (Invitrogen). For nonphosphorylable TDP-43 (SA-TDP-43) vector, primers containing the mutant substitution of TDP-43 serine 403/404 and 409/410 to alanine were used to mutagenize WT-TDP-43 (KOD-Plus-Mutagenesis kit; Toyobo, Osaka, Japan). The entry vector of WT- or SA-TDP-43 was transferred into pcDNA6.2/N-EmGFP-DEST Vector or pcDNA3.1/nV5-DEST using Gateway LR Clonase II enzyme mix (Invitrogen). The sequences of all constructs were verified using CEQ 8000 genetic analysis system (Beckman Coulter, Brea, CA).

Immunoblot analysis

For whole lysate analysis, NSC34 cells and primary cortical neurons were lysed in 2% SDS sample buffer. For analysis of protein solubility, cells cultured in 6-well plates were lysed in 100 μl of Tris (TS) buffer (50 mM Tris–HCl buffer, pH 7.5, 0.15 M NaCl, 5 mM EDTA, 5 mM EGTA, protein phosphatase inhibitors, and protease inhibitor cocktail). Lysates were sonicated and centrifuged at 100,000 ×*g* for 15 min. To prevent carryover, the pellets were washed with TS buffer, followed by sonication and centrifugation. TS-insoluble pellets were lysed in 50 μl of Triton-X100 (TX) buffer (TS buffer containing 1% Triton X-100), sonicated, and centrifuged at 100,000 *g* for 15 min. The pellets were washed with TX buffer, followed by sonication and centrifuge. TX-insoluble pellets were lysed in 50 μl of Sarkosyl (Sar) buffer (TS buffer containing 1% Sarkosyl), sonicated and centrifuged at 100,000 × g for 15 min. Sar-insoluble pellets were lysed in 25 μl of SDS sample buffer. After denaturation, 3 μl of each cell lysate was separated by SDS-PAGE (5%–20% gradient gel) and analyzed by western blotting with ECL Plus detection reagents (GE Healthcare, Buckinghamshire, UK). Primary antibodies used were as follows: anti-TDP-43 rabbit polyclonal antibody (1:1000, ProteinTech, Chicago, IL), anti-TDP-43 (405–414) rabbit polyclonal antibody (1:1000, Cosmo Bio Co. Ltd., Tokyo, Japan), anti-TDP-43 (phospho Ser403/404, Cosmo Bio) rabbit polyclonal antibody (1:1000, Cosmo Bio), anti-TDP-43 (phospho Ser409/410, Cosmo Bio) rabbit polyclonal antibody (1:1000, Cosmo Bio), anti-GAPDH mouse monoclonal antibody (1:2000, Temecula, CA), anti-GFP mouse monoclonal antibody (1:2000, MBL, Nagoya, Japan), and anti-V5 mouse monoclonal antibody (1:2000, Invitrogen).

Assay of ROS production

NSC34 cells to be treated with intended agents were incubated in 96-well plates with 5-(and-6)-chloromethyl-2′,7′-dichlorodihydro fluoresceindiacetate acetyl ester (CM-H2DCFDA) (Molecular Probes, Eugene, OR, USA) for 1 h. Oxidation in the cells was then measured in a multiple-plate reader (PowerscanHT, Dainippon Pharmaceutical, Japan) at excitation and emission wavelengths of 485 nm and 530 nm, respectively. The assays were carried out in 6 wells for each condition.

Immunocytochemistry

NSC34 cells and primary cortical neurons were fixed with 4% paraformaldehyde, incubated with PBS containing 0.2% Triton X-100 for 5 min, blocked, and incubated overnight with anti-TDP-43 rabbit polyclonal antibody (1:1000, ProteinTech), anti-TDP-43 (phospho Ser409/410) mouse monoclonal antibody (1:2000, Cosmo Bio) and anti-TIAR mouse monoclonal antibody (1:1000, BD Transduction Laboratories, Milan, Italy). After washing, samples were incubated with Alexa-488-conjugated goat anti-rabbit IgG (1:1000, Invitrogen) and Alexa-564-conjugated goat anti-mouse IgG (1:1000, Invitrogen) for 30 min, mounted with (Vector Laboratories, Inc. Burlingame, CA), then imaged with a laser conforcal microscope (Nikon A1, Nikon, Tokyo, Japan).

Time lapse analysis

NSC34 cells or mouse primary cortical neurons were grown on glass base dishes, transfected with GFP-WT-TDP-43, and treated with EA. GFP and phase contrast imaging was done every 10 min using a 40X objective lens on a laser scanning confocal microscope.

Cell viability analysis

The 3-(4,5-dimethylthiazol-2-yl)-5-(3-caboxymethoxyphenyl)-2-(4-sulfophenyl)-2H -tetrazolium (MTS)-based cell proliferation assay (MTS assay) was carried out using the CellTiter 96 Aqueous One Solution Cell Proliferation Assay (Promega, Madison, WI), according to the manufacturer's instructions. Absorbance at 490 nm was measured in a multiple-plate reader (PowerscanHT, Dainippon Pharmaceutical, Japan). The assays were carried out in 6 wells for each condition.

Statistical analysis

Statistical differences were analyzed by ANOVA and Bonferroni post hoc analyses for three group comparisons (SPSS version 15.0, SPSS Inc., Chicago, IL). Two-tailed $p<0.05$ was regarded as statistically significant.

Results

EA-mediated oxidative stress induces TDP-43 phosphorylation in NSC34 cells

To investigate the effect of oxidative stress on endogenous TDP-43, NSC34 cells were incubated for 12 h with EA, which is able to increase cellular oxidative stress through depletion of glutathione, (Keelan et al., 2001; Rizzardini et al., 2003). Immunoblots showed abnormal TDP-43-immunoreactive bands at 45 kDa, which suggests hyperphosphorylation of TDP-43, at EA concentration greater than 50 μM EA (Fig. 1A). The bands were immunopositive for phospho-TDP-43-specific (pTDP-43) antibodies at serine 403/404 and serine 409/410 (S403/404 and S409/410), that are seen in TDP-43 proteinopathies as pathological phosphorylation (Hasegawa et al., 2008) (Fig. 1A). In addition, phosphorylation of these TDP-43 sites was prevented by co-treatment with 2 mM NAC, a precursor of glutathione. Quantification of CM-H2DCFDA oxidation, a measure of ROS formation, showed that ROS productions was increased by EA treatment in a dose-dependent manner and was prevented by NAC (Fig. 1B). Since TDP-43 phosphorylation at S403/404 and S409/410 is exerted by CK1 and CK2 (Hasegawa et al., 2008), the effect of treatment with these inhibitors in combination with EA was examined. Both inhibitors prevented serine phosphorylation of TDP-43 in a dose-dependent manner, although CK1 inhibitor was more effective than CK2 inhibitor (Fig. 1C).

EA induces TDP-43 insolubilization and C-terminal fragmentation

To investigate the effect of oxidative stress on endogenous TDP-43 solubility, cells treated with 70 μM EA were extracted sequentially. In the immunoblots, the amount of TDP-43 in TS and TX fractions were significantly decreased, but the amount in Sar and SDS fractions were increased in a time-dependent manner (Fig. 2A). These phenomena were prevented in the presence of 2 mM NAC. Phosphorylated TDP-43 was increased in Sar fractions in a time-dependent manner and was detectable in SDS fractions 5 h after EA induction (Fig. 2A). In addition, long exposure of immunoblots with anti-TDP-43 antibody demonstrated that ~25 kDa C-terminal fragment (CTF) of TDP-43 in Sar and SDS fractions appeared evidently by EA induction, and the amount of TDP-43 CTF in SDS fraction was significantly increased at 5 h after EA induction compared with control (Fig. 2A, B).

EA induces cytoplasmic distribution of TDP-43

Immunocytochemistry showed that endogenous TDP-43 disappeared from the nucleus, translocated to the cytoplasm, and became phosphorylated at least in some population of NSC34 cells treated with 70 μM EA for 5 h, whereas this protein was localized in the nucleus and was not phosphorylated in untreated cells (Fig. 3A). Although the majority of cytoplasmic TDP-43 was diffusely distributed under EA treatment, it was also localized in stress granules (SGs), which were labeled with TIAR (Fig. 3A). The time lapse analysis of NSC43 cells expressing GFP-WT-TDP-43 demonstrated cytoplasmic distribution of TDP-43 in the majority of the cells treated with 70 μM EA, but TDP-43 consistently localized in the nucleus of cells co-treated with 2 mM NAC (Fig. 3B, C).

H_2O_2 induces C-terminal phosphorylation, C-terminal fragmentation, insolubilization, and cytoplasmic distribution of TDP-43

To confirm that the TDP-43 modifications are not induced by the specific toxicity of EA, we investigated the effects of H_2O_2, another

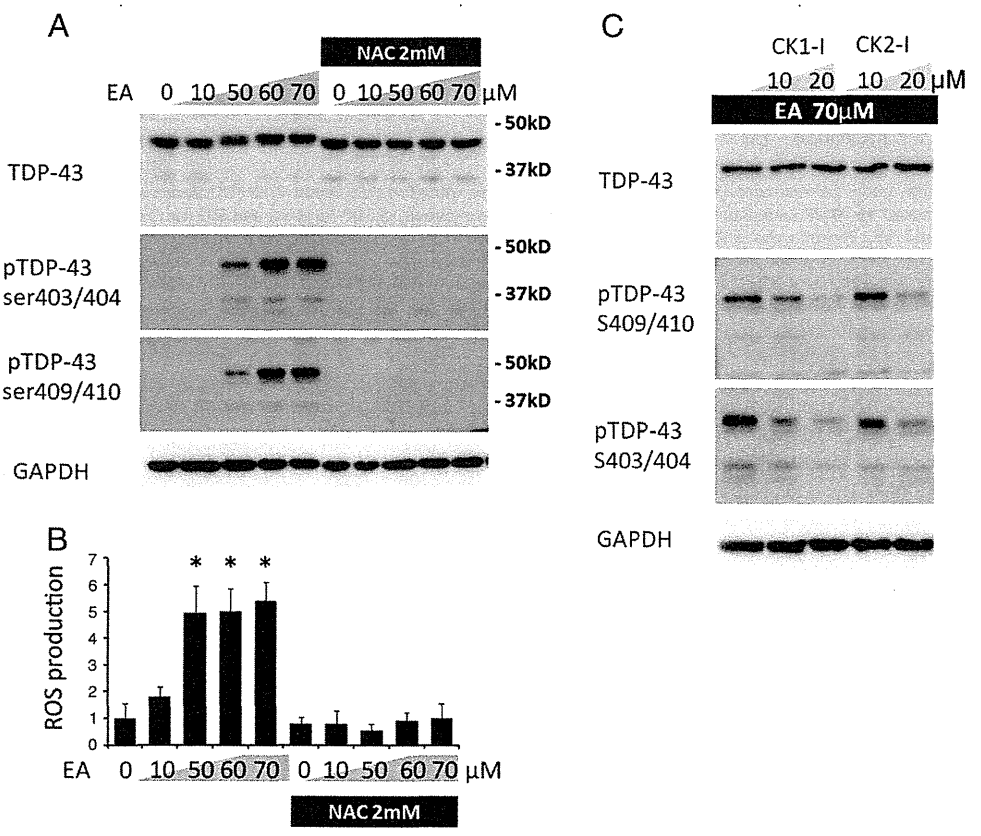

Fig. 1. TDP-43 phosphorylation induced by EA. (A) Immunoblots of NSC34 cells. EA induced TDP-43 C-terminal phosphorylation at S403/404 and S409/410 in a dose-dependent manner. The phosphorylation was prevented by 2 mM NAC. (B) Quantification of ROS by CM-H2DCFDA oxidative assay. The values relative to those of controls are shown. ROS production was increased by EA induction and suppressed by 2 mM NAC. Asterisk denotes significant difference from control ($p<0.0001$, $n=6$). Error bars indicate SD. (C) Immunoblots of NSC34 cells treated with 70 μM of EA. Casein kinase 1 and 2 inhibitors (CK1-I and CK2-I) both prevented the phosphorylation of TDP-43 in a dose-dependent manner.

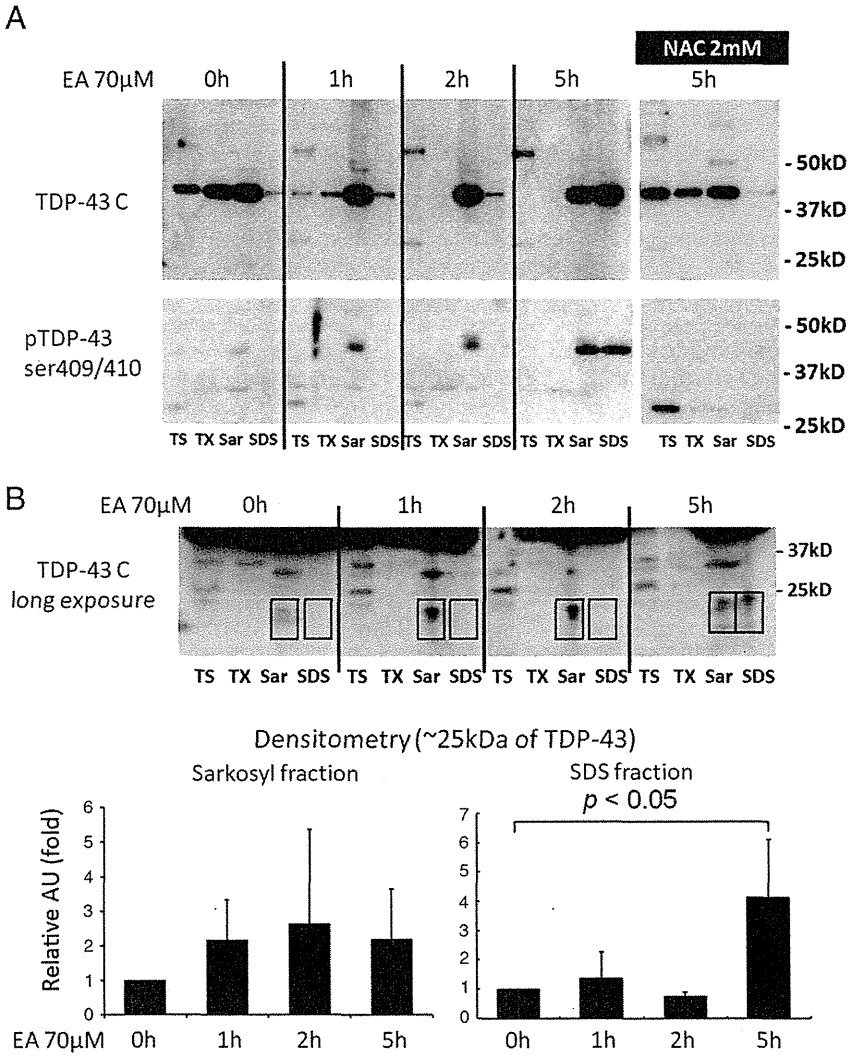

Fig. 2. Analysis of TDP-43 solubility under EA treatment. (A) Sequential extraction analysis using Tris (TS), Triton X100 (TX), Sarkosyl (Sar), and SDS buffers. The amount of TDP-43 in TS and TX fractions was decreased by 70 μM EA in a time-dependent manner, while the amount of TDP-43 in Sar and SDS fractions was increased by the treatment. These phenomena were prevented by 2 mM NAC. Phosphorylated TDP-43 (S409/410) was increased in Sar and SDS fractions in a time-dependent manner. (B) Densitometric quantitation of TDP-43C-terminal fragment (CTF). The relative intensities to controls are shown in arbitrary units (AU). Long exposure of immunoblots with anti-TDP-43 antibody (405–414) (TDP-43C) showed ~25 kDa C-terminal fragment (CTF) in Sar and SDS fractions. The amount of TDP-43 CTF was significantly increased in the SDS fraction at 5 h after EA induction (n = 3). Error bars indicate SD.

inducer of oxidative stress, on the modifications of TDP-43. Immunoblots of NSC34 cells showed that 10 mM H_2O_2 induced C-terminal phosphorylation and C-terminal fragmentation of TDP-43 (Fig. S4A). In the sequential extraction analysis of NSC34 cells, the amount of TDP-43 in TS and TX fractions was decreased by 10 mM H_2O_2, while that of TDP-43 in SDS fraction was increased by the treatment (Fig. S4B). The time lapse analysis of NSC34 cells expressing GFP-WT-TDP-43 showed that 10 mM H_2O_2 induced cytoplasmic distribution of TDP-43 (Fig. S4C).

EA induces C-terminal phosphorylation and cytoplasmic distribution of TDP-43 in primary cortical neurons

To investigate the effect of oxidative stress in neurons, 5-day in vivo (5 DIV) mouse primary cortical neurons were treated with EA for 5 h. Immunoblots showed that EA induced TDP-43 phosphorylation at S403/404 and S409/410 in a dose-dependent manner, and 2 mM NAC prevented the phosphorylation (Fig. 4A). In the time lapse analysis of neurons expressing GFP-WT-TDP-43, TDP-43 was distributed in the cytoplasm in the presence of 30 μM EA (Fig. 4B).

C-terminal phosphorylation of TDP-43 is not mandatory for its insolubilization or cytoplasmic distribution under EA

Since C-terminal phosphorylation of TDP-43 was accompanied by insolubilization and distribution to the cytoplasm in response to oxidative stress, we investigated the effect of C-terminal phosphorylation of TDP-43 using a nonphosphorylable TDP-43 (SA-TDP-43) mutant which contains serine to alanine substitutions at 403/404 and 409/410 (Fig. 5A). We used N-terminal tagged TDP-43, since C-terminal tagged TDP-43 was not detected by anti-pTDP-43 antibody in the immunoblots even under conditions of oxidative stress sufficient to phosphorylate endogenous TDP-43 (Fig. S1). As was seen with WT-TDP-43 under normal conditions, GFP-tagged and V5-tagged SA-TDP-43 were located in the nucleus (Fig. S2). In the immunoblots, endogenous and GFP-WT-TDP-43 were phosphorylated in the presence of 70 μM EA, but GFP-SA-TDP-43 was not phosphorylated even at an EA concentration of 70 μM (Fig. 5B). The time lapse analysis of NSC34 cells demonstrated that GFP-SA-TDP-43 translocated to the cytoplasm (Fig. 6A). The proportion of the cells with cytoplasmic distribution of TDP-43 under oxidative stress was not

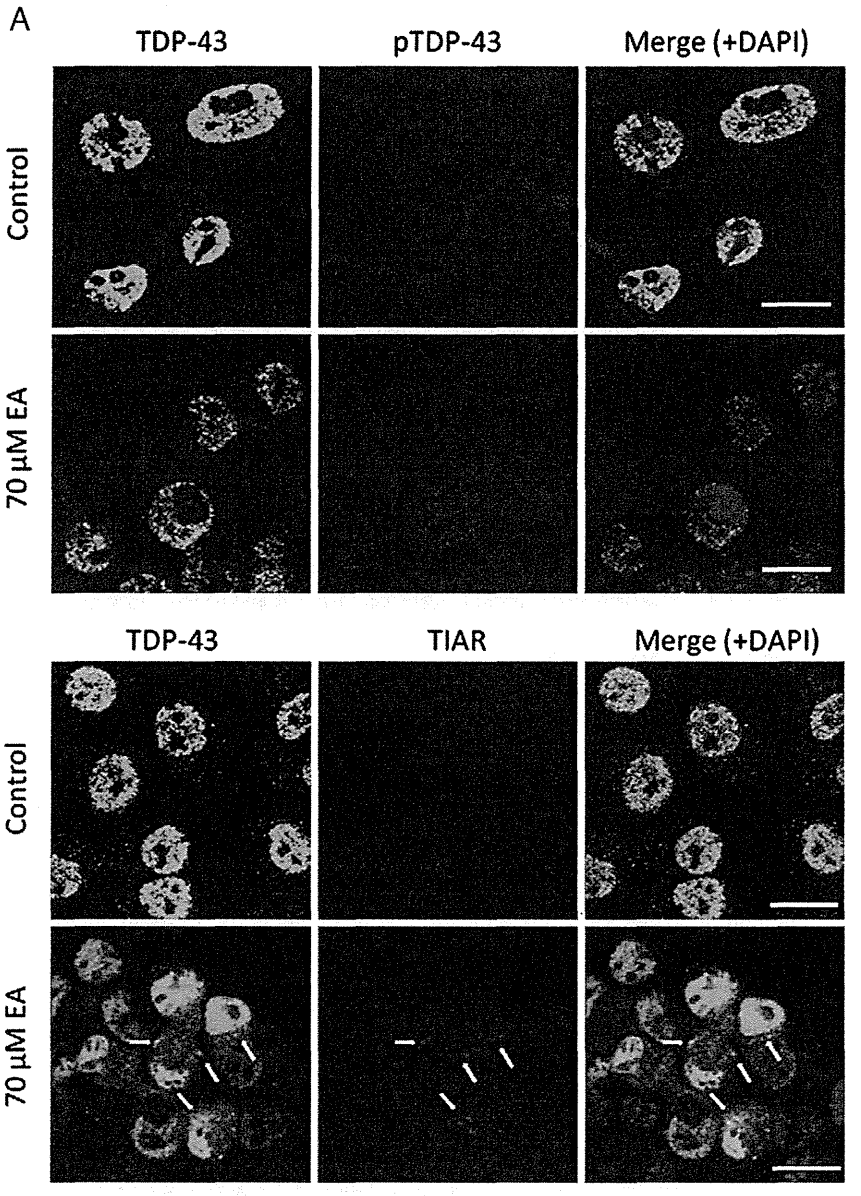

Fig. 3. Cytoplasmic distribution of TDP-43 induced by EA. (A) Immunocytochemistry of NSC34 cells. Cells were stained with anti-TDP-43 antibody (green), anti-phospho-specific TDP-43 (pTDP-43) (S409/410) or anti-TIAR antibody (red), and DAPI (blue). EA treatment (70 μM, 5 h) induced translocation of TDP-43 from the nucleus to the cytoplasm in NSC34 cells. Cytoplasmic TDP-43 was immunopositive for pTDP-43 antibody. In the control cells TDP-43 localized in the nucleus without phosphorylation. TDP-43 co-localized with stress granule marker, TIAR under EA treatment, although the majority of cytoplasmic TDP-43 was diffusely distributed. Arrows indicate stress granules. Scale bars represent 10 μm. (B) Time lapse analysis of NSC43 cells expressing GFP-WT-TDP-43. GFP and phase contrast images showed that TDP-43 was distributed to the cytoplasm when exposed to 70 μM EA, but this distribution was prevented by 2 mM of NAC. (C) The proportion of cells with cytoplasmic distribution of TDP-43 (cells with cyto-TDP) in the GFP-TDP-43 expressing cells 0 h or 5 h after EA induction without or with NAC treatment. Three areas per sample were measured. Error bars indicate SD.

different between WT- and SA-TDP-43 (Fig. 6B). Sequential extraction of NSC34 cells was performed using V5-tagged TDP-43 vectors, since the Sar-insoluble fraction of GFP-TDP-43 was abundant even in the absence of oxidative stress (data not shown). The amount of Sar-insoluble fraction of SA-TDP-43 detected was the same as was seen with WT-TDP-43. (Fig. 7A, B). These findings indicate that phosphorylation is not necessary for oxidative-stress mediated insolubilization and cytoplasmic distribution of TDP-43. Next, we performed MTS assay of NSC34 cells to investigate the effect of TDP-43 and its modifications on the cell viability. The results showed that no significant difference in the viability among the cells expressing GFP-mock, GFP-WT- and GFP-SA-TDP-43, either 0 h or 5 h after EA induction (Fig. S3).

Discussion

Post-translational modifications of TDP-43 such as C-terminal phosphorylation, insolubilization, C-terminal fragmentation, and cytoplasmic distribution are pathological hallmarks of TDP-43 proteinopathies (Arai et al., 2006; Hasegawa et al., 2008; Neumann et al., 2006). TDP-43 with defective nuclear localization signal (NLS) was shown to promote cytoplasmic aggregation, C-terminal phosphorylation, and C-terminal fragmentation of TDP-43 in cell-based studies (Nonaka et al., 2009a; Winton et al., 2008). In addition, overexpression of TDP-43 CTF lead to phosphorylation and formation of cytoplasmic aggregates (Igaz et al., 2009; Nonaka et al., 2009b). Although these observations suggest that the cytoplasmic localization

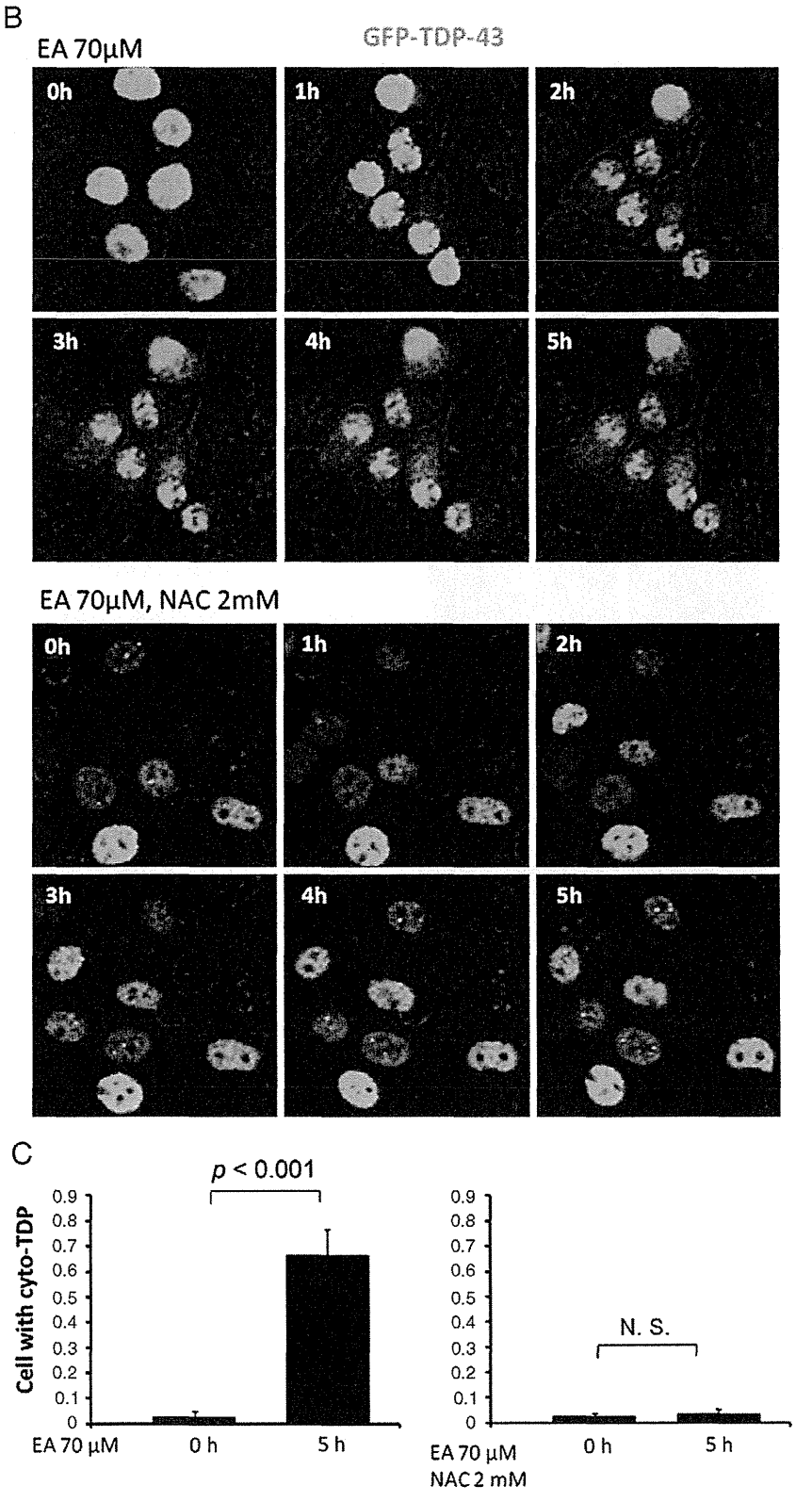

Fig. 3 (*continued*).

or fragmentation of TDP-43 facilitates its pathological modification such as aggregation and phosphorylation, the initial cause of these modifications in TDP-43 proteinopathies has not been fully elucidated. Some studies have demonstrated that artificial axonal damage induces transient cytoplasmic distribution of TDP-43 in motor neurons (Moisse et al., 2009; Sato et al., 2009), indicating that the pathological distribution of TDP-43 may result from the cellular response to neuronal injury or axonal obstruction. However, in these affected neurons, aggregation, C-terminal fragmentation and phosphorylation of TDP-43 were not observed. Furthermore, zinc-induced nuclear

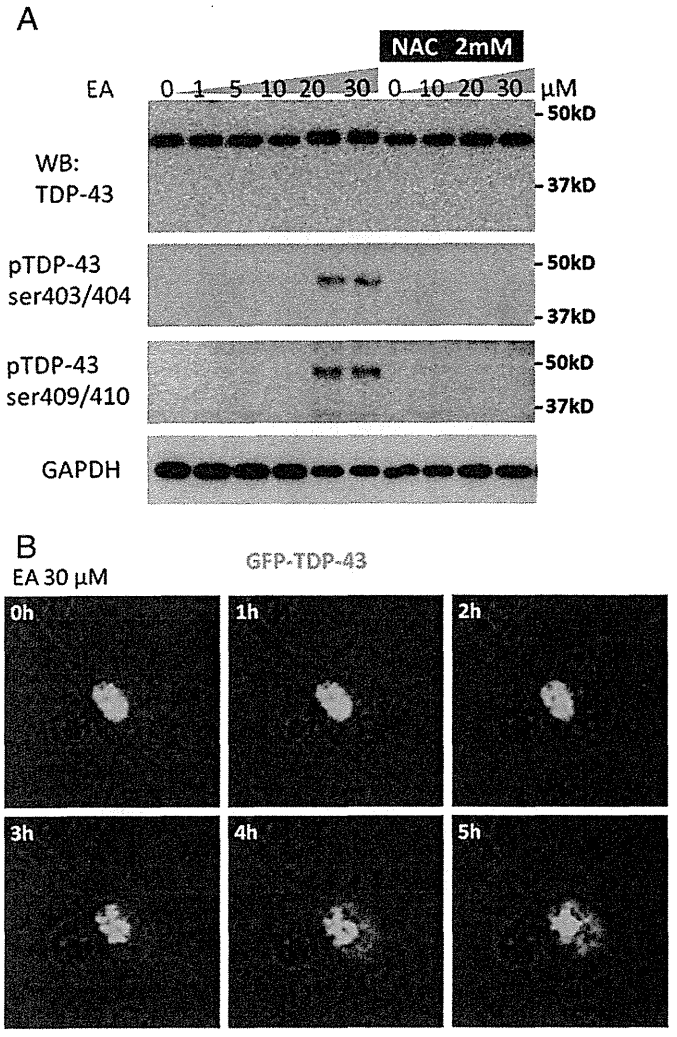

Fig. 4. TDP-43 modification induced by EA in primary cortical neuron. (A) Immunoblots of primary cortical neurons. EA induced TDP-43 phosphorylation at S403/404 and S409/410 in a dose-dependent manner, and this was prevented by 2 mM NAC. (B) Time lapse analysis of neurons expressing GFP-WT-TDP-43. TDP-43 in primary cultures was distributed to the cytoplasm in the presence of 30 μM EA.

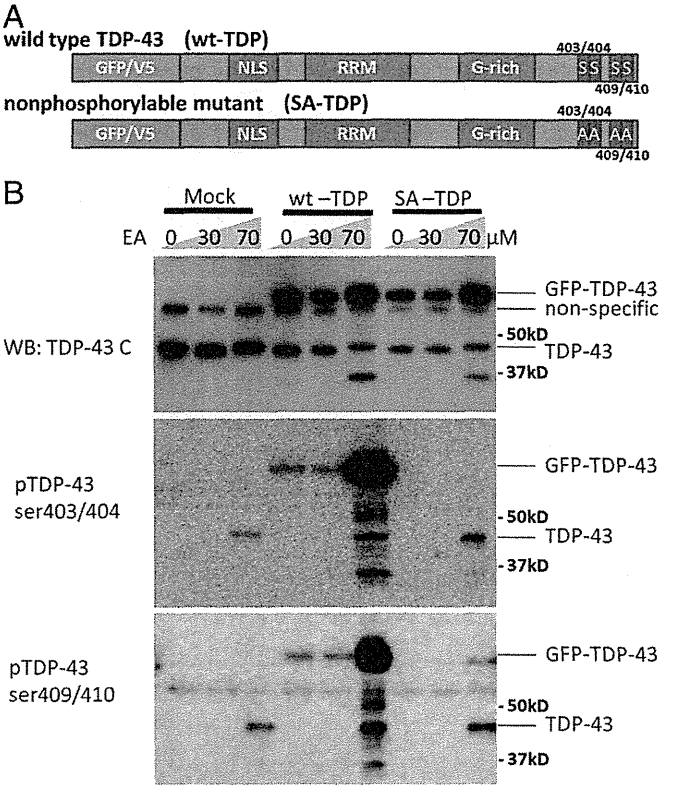

Fig. 5. Nonphosphorylable mutant of TDP-43. (A) Structures of WT- and SA-TDP-43 vectors. SA-TDP-43 contains serine to alanine substitutions at 403/404 and 409/410. (B) Immunoblots of NSC34 cells expressing GFP-WT- or GFP-SA-TDP-43. Endogenous and GFP-WT-TDP-43 were phosphorylated at both 403/404 and 409/410 by 70 μM EA, but GFP-SA-TDP-43 was not phosphorylated by the treatment.

inclusion formations have also been observed in SY5Y cells, but not C-terminal fragmentation or phosphorylation of TDP-43 (Caragounis et al., 2010).

In the present study, we demonstrated that a compound that induces cellular glutathione depletion, EA induced C-terminal phosphorylation of TPD-43 at S403/404 and S409/410 in NSC34 cells and mouse primary cortical neurons, and that NAC completely prevented this phosphorylation. In addition, inhibitors of both CK1 and CK2 also prevented the phosphorylation in a dose-dependent manner. These findings indicate that C-terminal phosphorylation of TDP-43 occurs as a consequence of oxidative stress induced by glutathione depletion and is mediated by CK1 and CK2. Furthermore, the sequential extract analysis showed that EA reduced the solubility of TDP43 and increased the amount of ~25 kDa CTF in the Sar-insoluble fraction. Additionally, EA also induced cytoplasmic distribution of TDP-43 in NSC34 cells and primary cortical neurons. The time lapse analysis showed that cytoplasmic distribution of TDP-43 was seen in the majority of NSC34 cells. Although the immunocytochemistry of TDP-43 demonstrated that cytoplasmic distribution of TDP-43 were observed only in a certain population of NSC34 cells treated with EA, this is likely due to the fact that most of damaged cells could not stay adherent to the plate during the fixation. Previous reports indicated that severe level of oxidative stress may result in apoptotic cell death, and that caspase activation induces C-terminal fragmentation of TDP-43 (Dormann et al., 2009; Zhang et al., 2007). These observations do not exclude the possibility that caspase activation contributes to TDP-43 modifications that were observed under EA treatment. The results of the present study demonstrated that H_2O_2, another inducer of oxidative stress, also causes C-terminal phosphorylation, fragmentation, insolubilization, and cytoplasmic distribution of TDP-43 as observed under EA exposure. These data suggest that oxidative stress is involved in the process of the pathological TDP-43 modifications seen in TDP-43 proteinopathies. The facts that oxidative stress is associated with aging-related disorders (Frederickson et al., 2005; Migliore, 2005) and that TDP-43 proteinopathies are aging process-related diseases may support our assumption that oxidative stress possibly mediates TDP-43 modification. A high frequency of abnormal TDP-43 pathology such as C-terminal phosphorylation has been found not only in patients with TDP-43 proteinopathies but also in patients with other neurodegenerative disease such as AD, DLB, and HD (Arai et al., 2010). Since numerous studies have demonstrated increased oxidative cellular damage in these conditions (Butterfield et al., 2007; Lovell and Markesbery, 2007; Nunomura et al., 2002), oxidative stress may be a cause of pathological TDP-43 modification in various neurodegenerative disorders.

Several studies demonstrated that TDP-43 is involved in SGs under cellular stresses including arsenite treatment and heat shock (Colombrita et al., 2009; Liu-Yesucevitz et al., 2010; McDonald et al., 2011; Nishimoto et al., 2010). Although TDP-43 was seen as a component of SGs under EA treatment, majority of cytoplasmic TDP-43 was independent of SGs and was diffusely distributed. These findings suggest that there is SG-independent mechanism for cytoplasmic distribution of TDP-43 under oxidative stress induced by glutathione depletion.

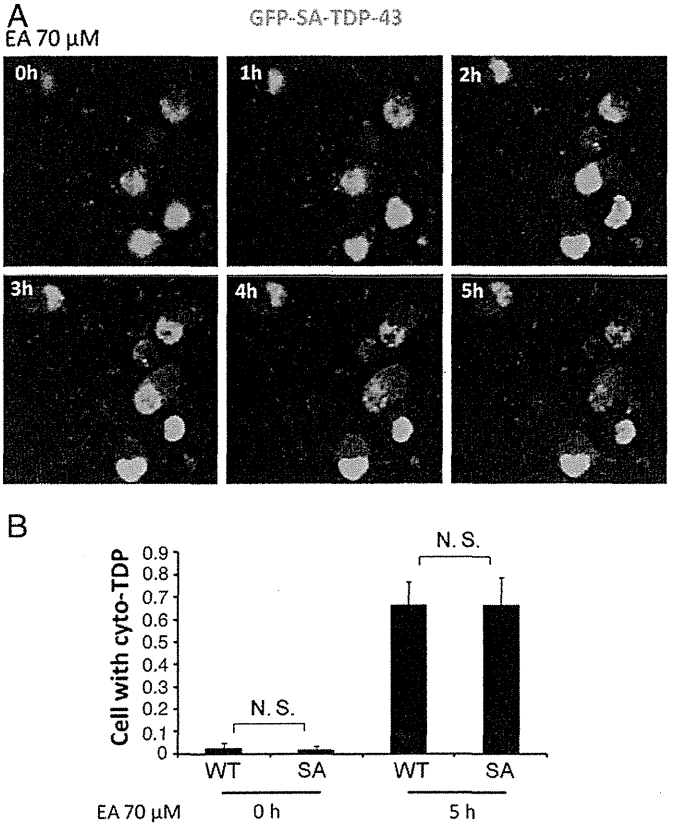

Fig. 6. The effect of C-terminal phosphorylation on TDP-43 distribution. (A) Time lapse analysis of NSC34 cells expressing GFP-SA-TDP-43. GFP-SA-TDP-43 was distributed to the cytoplasm by 70 μM of EA. (B) The proportion of cells with cytoplasmic distribution of TDP-43 (cells with cyto-TDP) in the GFP-TDP-43 expressing cells. The proportion of cells with cyto-TDP was not different between WT- and SA-TDP-43, either 0 h or 5 h after EA induction. Three areas per sample were measured. Error bars indicate SD.

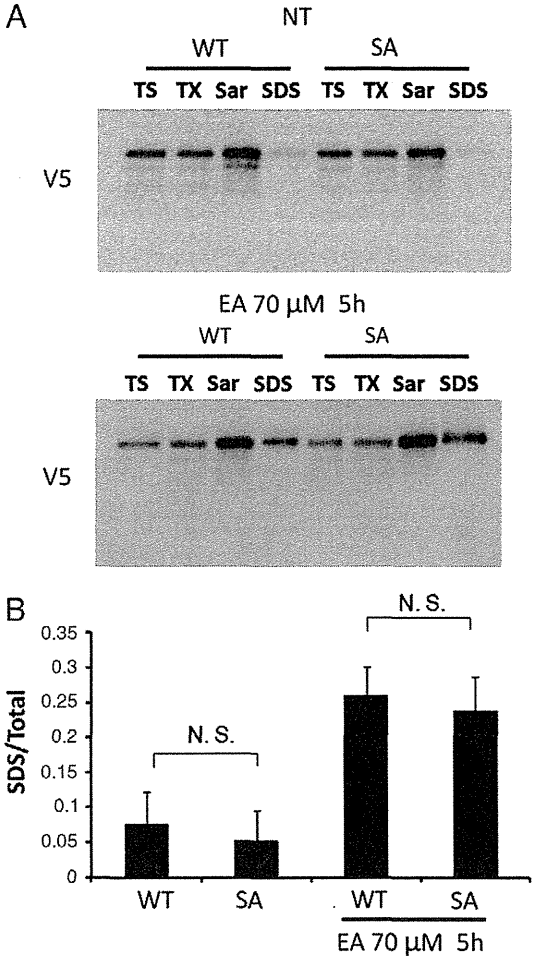

Fig. 7. The effect of C-terminal phosphorylation on TDP-43 solubility. (A) Sequential extraction of NSC34 cells expressing V5-WT- or V5-SA-TDP-43. (B) Densitometric quantitation of Sar-insoluble V5-TDP-43. Ratio of Sar-insoluble fraction from the whole fraction did not differ between WT- and SA-TDP-43 with or without 70 μM EA. Three independent experiments were performed. Error bars indicate SD.

In the present study, S403/404 and S409/410 of TDP-43 were phosphorylated together with insolubilization and cytoplasimic distribution of the protein. The hyperphosphorylation of disease marker proteins is a common feature of neurodegenerative disorders, and its relation to the pathogenesis has been intensively investigated: Tau in AD; huntingtin in HD; and alfa-synuclein in PD and DLB (Ballatore et al., 2007; Fujiwara et al., 2002; Gu et al., 2009). A number of studies have demonstrated that disease-specific phosphorylation of these marker proteins modulates aggregation and potentially influences disease pathogenesis (Azeredo da Silveira et al., 2009; Gu et al., 2009). In the present study, there was no difference between wild type and non-phosphorylable TDP-43 in the degree of insolubilization and cytoplasmic translocation under oxidative stress conditions, suggesting that C-terminal phosphorylation of TDP-43 is not mandatory for aggregation or abnormal intracellular distribution. In support with our findings, there is a study demonstrating that C-terminal phosphorylation of TDP-43 is not substantially required for the cytoplasmic aggregation (Brady et al., 2010). In addition, our results show that C-terminal tags interfere with the detection of TDP-43 phosphorylation, providing a cautionary note for cell-based and animal studies of TDP-43 with a C-terminal tag.

We further examined whether the pathological modifications of TDP-43 contribute to cell vulnerability to glutathione depletion. In the analysis of MTS assay, the viabilities of NSC34 cells were decreased by EA treatment. Although GFP-WT-TDP-43 was fully phosphorylated, insolubilized and distributed to cytoplasm in the cells treated with EA, there was no significant difference in the viability between the cells expressing GFP-mock and GFP-WT-TDP-43. In addition, the viability of NSC34 cells expressing GFP-SA-TDP-43 was not different from that of the cells expressing GFP-WT-TDP-43. These findings suggest that TDP-43 modification may not affect cell viability under oxidative stress induced by glutathione depletion.

In conclusion, we demonstrated that oxidative stress induced by glutathione depletion instigated TDP-43 modifications including C-terminal phosphorylation, insolubilization, C-terminal fragmentation and cytoplasmic distribution, and that these changes reproduce the pathological features of TDP-43 proteinopathies and other neurodegenerative diseases such as AD.

Supplementary materials related to this article can be found online at doi:10.1016/j.nbd.2011.12.002.

Funding

Funding: This work was supported by a Center-of-Excellence (COE) grant, a Grant-in-Aid for Scientific Research on Innovated Areas "Foundation of Synapse and Neurocircuit Pathology," and Grant-in-Aids from Ministry of Education, Culture, Sports, Science, and Technology of Japan; grants from the Ministry of Health, Labor and Welfare of Japan; and Core Research for Evolutional Science and Technology (CREST) of the Japan Science and Technology Agency (JST).

References

Abe, K., et al., 1995. Induction of nitrotyrosine-like immunoreactivity in the lower motor neuron of amyotrophic lateral sclerosis. Neurosci. Lett. 199, 152–154.

Abe, K., et al., 1997. Upregulation of protein-tyrosine nitration in the anterior horn cells of amyotrophic lateral sclerosis. Neurol. Res. 19, 124–128.
Amador-Ortiz, C., et al., 2007. TDP-43 immunoreactivity in hippocampal sclerosis and Alzheimer's disease. Ann. Neurol. 61, 435–445.
Arai, T., et al., 2006. TDP-43 is a component of ubiquitin-positive tau-negative inclusions in frontotemporal lobar degeneration and amyotrophic lateral sclerosis. Biochem. Biophys. Res. Commun. 351, 602–611.
Arai, T., et al., 2009. Phosphorylated TDP-43 in Alzheimer's disease and dementia with Lewy bodies. Acta Neuropathol. 117, 125–136.
Arai, T., et al., 2010. Phosphorylated and cleaved TDP-43 in ALS, FTLD and other neurodegenerative disorders and in cellular models of TDP-43 proteinopathy. Neuropathology 30, 170–181.
Ayala, Y.M., et al., 2005. Human, Drosophila, and C.elegans TDP43: nucleic acid binding properties and splicing regulatory function. J. Mol. Biol. 348, 575–588.
Ayala, Y.M., et al., 2008. TDP-43 regulates retinoblastoma protein phosphorylation through the repression of cyclin-dependent kinase 6 expression. Proc. Natl. Acad. Sci. U. S. A. 105, 3785–3789.
Azeredo da Silveira, S., et al., 2009. Phosphorylation does not prompt, nor prevent, the formation of alpha-synuclein toxic species in a rat model of Parkinson's disease. Hum. Mol. Genet. 18, 872–887.
Ballatore, C., et al., 2007. Tau-mediated neurodegeneration in Alzheimer's disease and related disorders. Nat. Rev. Neurosci. 8, 663–672.
Beal, M.F., et al., 1997. Increased 3-nitrotyrosine in both sporadic and familial amyotrophic lateral sclerosis. Ann. Neurol. 42, 644–654.
Brady, O.A., et al., 2010. Regulation of TDP-43 aggregation by phosphorylation and p62/SQSTM1. J. Neurochem. 116, 248–259.
Buratti, E., et al., 2005. TDP-43 binds heterogeneous nuclear ribonucleoprotein A/B through its C-terminal tail: an important region for the inhibition of cystic fibrosis transmembrane conductance regulator exon 9 splicing. J. Biol. Chem. 280, 37572–37584.
Buratti, E., et al., 2010. Nuclear factor TDP-43 can affect selected microRNA levels. FEBS J. 277, 2268–2281.
Butterfield, D.A., et al., 2007. Roles of amyloid beta-peptide-associated oxidative stress and brain protein modifications in the pathogenesis of Alzheimer's disease and mild cognitive impairment. Free Radic. Biol. Med. 43, 658–677.
Caragounis, A., et al., 2010. Zinc induces depletion and aggregation of endogenous TDP-43. Free Radic. Biol. Med. 48, 1152–1161.
Colombrita, C., et al., 2009. TDP-43 is recruited to stress granules in conditions of oxidative insult. J. Neurochem. 111, 1051–1061.
Dormann, D., et al., 2009. Proteolytic processing of TAR DNA binding protein-43 by caspases produces C-terminal fragments with disease defining properties independent of progranulin. J. Neurochem. 110, 1082–1094.
Ferrante, R.J., et al., 1997. Evidence of increased oxidative damage in both sporadic and familial amyotrophic lateral sclerosis. J. Neurochem. 69, 2064–2074.
Frederickson, C.J., et al., 2005. The neurobiology of zinc in health and disease. Nat. Rev. Neurosci. 6, 449–462.
Fujiwara, H., et al., 2002. alpha-Synuclein is phosphorylated in synucleinopathy lesions. Nat. Cell Biol. 4, 160–164.
Geser, F., et al., 2008. Pathological TDP-43 in parkinsonism-dementia complex and amyotrophic lateral sclerosis of Guam. Acta Neuropathol. 115, 133–145.
Gu, X., et al., 2009. Serines 13 and 16 are critical determinants of full-length human mutant huntingtin induced disease pathogenesis in HD mice. Neuron 64, 828–840.
Hasegawa, M., et al., 2007. TDP-43 is deposited in the Guam parkinsonism-dementia complex brains. Brain 130, 1386–1394.
Hasegawa, M., et al., 2008. Phosphorylated TDP-43 in frontotemporal lobar degeneration and amyotrophic lateral sclerosis. Ann. Neurol. 64, 60–70.
Igaz, L.M., et al., 2009. Expression of TDP-43 C-terminal Fragments in Vitro Recapitulates Pathological Features of TDP-43 Proteinopathies. J. Biol. Chem. 284, 8516–8524.
Iguchi, Y., et al., 2009. TDP-43 depletion induces neuronal cell damage through dysregulation of Rho family GTPases. J. Biol. Chem. 284, 22059–22066.
Keelan, J., et al., 2001. Quantitative imaging of glutathione in hippocampal neurons and glia in culture using monochlorobimane. J. Neurosci. Res. 66, 873–884.
Liu-Yesucevitz, L., et al., 2010. Tar DNA binding protein-43 (TDP-43) associates with stress granules: analysis of cultured cells and pathological brain tissue. PLoS One 5, e13250.
Lovell, M.A., Markesbery, W.R., 2007. Oxidative DNA damage in mild cognitive impairment and late-stage Alzheimer's disease. Nucleic Acids Res. 35, 7497–7504.
McDonald, K.K., et al., 2011. TAR DNA-binding protein 43 (TDP-43) regulates stress granule dynamics via differential regulation of G3BP and TIA-1. Hum. Mol. Genet. 20, 1400–1410.
Migliore, L., 2005. Searching for the role and the most suitable biomarkers of oxidative stress in Alzheimer's disease and in other neurodegenerative diseases. Neurobiol. Aging 26, 587–595.
Moisse, K., et al., 2009. Divergent patterns of cytosolic TDP-43 and neuronal progranulin expression following axotomy: implications for TDP-43 in the physiological response to neuronal injury. Brain Res. 1249, 202–211.
Neumann, M., et al., 2006. Ubiquitinated TDP-43 in frontotemporal lobar degeneration and amyotrophic lateral sclerosis. Science 314, 130–133.
Nishimoto, Y., et al., 2010. Characterization of alternative isoforms and inclusion body of the TAR DNA-binding protein-43. J. Biol. Chem. 285, 608–619.
Nonaka, T., et al., 2009a. Phosphorylated and ubiquitinated TDP-43 pathological inclusions in ALS and FTLD-U are recapitulated in SH-SY5Y cells. FEBS Lett. 583, 394–400.
Nonaka, T., et al., 2009b. Truncation and pathogenic mutations facilitate the formation of intracellular aggregates of TDP-43. Hum. Mol. Genet. 18, 3353–3364.
Nunomura, A., et al., 2002. Neuronal RNA oxidation is a prominent feature of dementia with Lewy bodies. Neuroreport 13, 2035–2039.
Polymenidou, M., et al., 2011. Long pre-mRNA depletion and RNA missplicing contribute to neuronal vulnerability from loss of TDP-43. Nat. Neurosci. 14, 459–468.
Rizzardini, M., et al., 2003. Mitochondrial dysfunction and death in motor neurons exposed to the glutathione-depleting agent ethacrynic acid. J. Neurol. Sci. 207, 51–58.
Sato, T., et al., 2009. Axonal ligation induces transient redistribution of TDP-43 in brainstem motor neurons. Neuroscience 164, 1565–1578.
Sephton, C.F., et al., 2011. Identification of neuronal RNA targets of TDP-43-containing ribonucleoprotein complexes. J. Biol. Chem. 286, 1204–1215.
Shaw, I.C., et al., 1995. Studies on cellular free radical protection mechanisms in the anterior horn from patients with amyotrophic lateral sclerosis. Neurodegeneration 4, 391–396.
Strong, M.J., et al., 2007. TDP43 is a human low molecular weight neurofilament (hNFL) mRNA-binding protein. Mol. Cell. Neurosci. 35, 320–327.
Tollervey, J.R., et al., 2011. Characterizing the RNA targets and position-dependent splicing regulation by TDP-43. Nat. Neurosci. 14, 452–458.
Wang, I.F., et al., 2002. Higher order arrangement of the eukaryotic nuclear bodies. Proc. Natl. Acad. Sci. U. S. A. 99, 13583–13588.
Wang, H.Y., et al., 2004. Structural diversity and functional implications of the eukaryotic TDP gene family. Genomics 83, 130–139.
Winton, M.J., et al., 2008. Disturbance of nuclear and cytoplasmic TAR DNA-binding protein (TDP-43) induces disease-like redistribution, sequestration, and aggregate formation. J. Biol. Chem. 283, 13302–13309.
Zhang, Y.J., et al., 2007. Progranulin mediates caspase-dependent cleavage of TAR DNA binding protein-43. J. Neurosci. 27, 10530–10534.

OPEN ACCESS Freely available online

PLOS ONE

dnc-1/dynactin 1 Knockdown Disrupts Transport of Autophagosomes and Induces Motor Neuron Degeneration

Kensuke Ikenaka[1], Kaori Kawai[1], Masahisa Katsuno[1], Zhe Huang[1], Yue-Mei Jiang[1], Yohei Iguchi[1], Kyogo Kobayashi[2], Tsubasa Kimata[2], Masahiro Waza[1], Fumiaki Tanaka[1], Ikue Mori[2], Gen Sobue[1,3]*

1 Department of Neurology, Nagoya University Graduate School of Medicine, Nagoya, Japan, **2** Group of Molecular Neurobiology, Nagoya University Graduate School of Science, Nagoya, Japan, **3** Core Research for Evolutional Science and Technology (CREST), Japan Science and Technology Agency (JST), Saitama, Japan

Abstract

Amyotrophic lateral sclerosis (ALS) is a fatal neurodegenerative disease characterized by the progressive loss of motor neurons. We previously showed that the expression of dynactin 1, an axon motor protein regulating retrograde transport, is markedly reduced in spinal motor neurons of sporadic ALS patients, although the mechanisms by which decreased dynactin 1 levels cause neurodegeneration have yet to be elucidated. The accumulation of autophagosomes in degenerated motor neurons is another key pathological feature of sporadic ALS. Since autophagosomes are cargo of dynein/dynactin complexes and play a crucial role in the turnover of several organelles and proteins, we hypothesized that the quantitative loss of dynactin 1 disrupts the transport of autophagosomes and induces the degeneration of motor neuron. In the present study, we generated a *Caenorhabditis elegans* model in which the expression of DNC-1, the homolog of dynactin 1, is specifically knocked down in motor neurons. This model exhibited severe motor defects together with axonal and neuronal degeneration. We also observed impaired movement and increased number of autophagosomes in the degenerated neurons. Furthermore, the combination of rapamycin, an activator of autophagy, and trichostatin which facilitates axonal transport dramatically ameliorated the motor phenotype and axonal degeneration of this model. Thus, our results suggest that decreased expression of dynactin 1 induces motor neuron degeneration and that the transport of autophagosomes is a novel and substantial therapeutic target for motor neuron degeneration.

Citation: Ikenaka K, Kawai K, Katsuno M, Huang Z, Jiang Y-M, et al. (2013) *dnc-1/dynactin 1* Knockdown Disrupts Transport of Autophagosomes and Induces Motor Neuron Degeneration. PLoS ONE 8(2): e54511. doi:10.1371/journal.pone.0054511

Editor: Udai Pandey, Lousiana State University Health Sciences Center, United States of America

Received October 2, 2012; **Accepted** December 12, 2012; **Published** February 7, 2013

Funding: This work was supported by Grants-in-Aid for Scientific Research and Global COE Program from the Ministry of Education, Culture, Sports, Science, and Technology, Grants-in-Aid for Scientific Research from the Ministry of Health, Labor, and Welfare, a Grant-in-Aid for Scientific Research on Innovated Areas "Foundation of Synapse and Neurocircuit Pathology", and Core Research for Evolutional Science and Technology (CREST) from Japan Science and Technology Agency (JST). The funders had no role in study design, data collection and analysis, decision to publish, or preparation of the manuscript.

Competing Interests: The authors have declared that no competing interests exist.

* E-mail: sobueg@med.nagoya-u.ac.jp

Introduction

Autophagy is one of the major cellular systems that regulate protein degradation and organelle turnover in physiological and pathological conditions [1], and it is an essential quality control system for proteins in post-mitotic neurons that need to eliminate abnormal proteins and organelles for their proper function and survival [2,3]. It is well known that the dysregulation of autophagy causes neurodegeneration [4,5] and that the abnormal accumulation of autophagosomes is observed in several neurodegenerative diseases [6–9]. Particularly, intensified immunoreactivity for microtubule-associated protein 1 light chain 3 (LC3), which is a marker of autophagosome, is often observed in the spinal motor neurons of amyotrophic lateral sclerosis (ALS) patients [8,10]. Electron microscopy of the motor neurons of ALS patients shows an increased number of autophagosomes surrounded by a double-membrane that contain sequestered cytoplasmic organelles, e.g., mitochondria [8]. Although these observations suggest the possibility that autophagy is upregulated to protect neurons from increased amounts of aggregated proteins and/or damaged organelles, it is also possible that the accumulation of autophagosomes due to dysregulated autophagy leads to neurodegeneration.

One possible mechanism for the accumulation of autophagosomes in degenerated neurons is the disruption of the cellular transport system, given that autophagosomes are cargo that moves bidirectionally along microtubules, which is powered by the kinesin family of motor proteins and dynein/dynactin complexes [11,12]. We previously investigated the motor neuron-specific gene expression profile of sporadic ALS (SALS), which accounts for more than 90% of ALS, and found that the expression of dynactin 1, which is a key member of the dynactin family, is markedly decreased in the spinal motor neurons of SALS patients [9]. The decreased expression of dynactin 1 was also verified quantitatively using *in situ* hybridization analysis of tissues from SALS patients [13]. By contrast, the expression of other motor proteins including the kinesin family, which are responsible for anterograde transport and dyneins, which are responsible for retrograde transport was not significantly changed. Thus, we hypothesized that the decreased expression of dynactin 1 results in the disrupted transport of autophagosomes and thus attenuates the protective effects of autophagy against neurodegeneration.

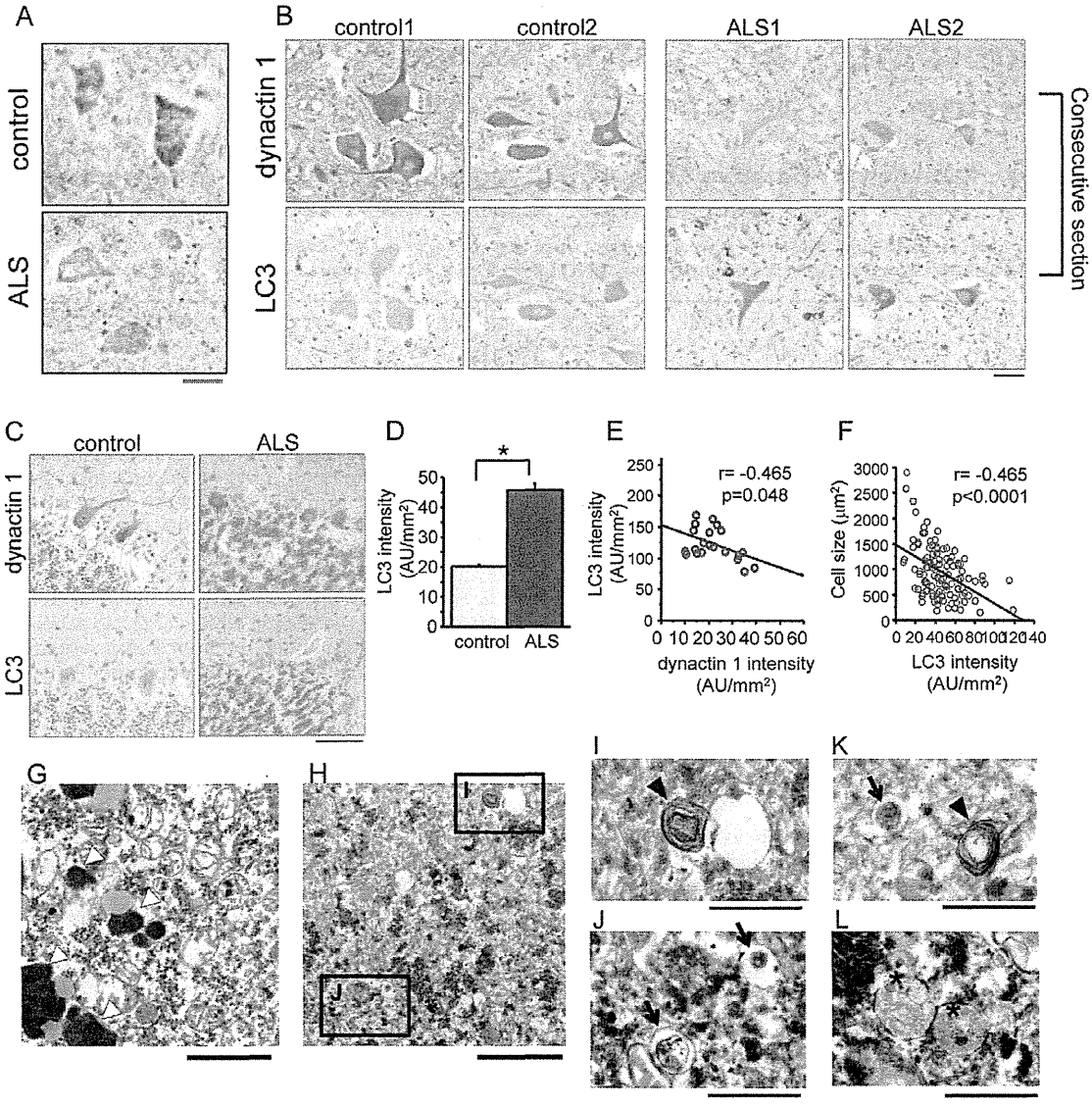

Figure 1. Dysregulated expression of dynactin 1 and the accumulation of autophagosomes in SALS patients. (*A*) Representative *in situ* hybridization for *DCTN1* in the spinal cords of control and ALS patients. (*B, C*) Representative immunohistochemistry for dynactin 1 and microtubule-associated protein 1 light chain 3 alpha (LC3) on consecutive spinal cord (*B*) and cerebellar (*C*) sections from control and ALS patients. (*D*) Quantification of the signal intensity of LC3 in anterior horn neurons of the spinal cord (n = 20 sections from 4 patients for each group). (*E*) Correlation between LC3 intensity and the expression of *DCTN1* in individual motor neurons from SALS patients (n = 12 consecutive sections from 3 SALS patients). (*F*) Correlation between the intensity of LC3 immunoreactivity and the size of motor neurons in SALS patients (n = 20 sections from 4 patients). (*G–L*) Electron microscopy images of spinal motor neurons. Representative lower magnification image of a motor neuron from a control patient (*G*) and lower (*H*) and higher magnification images (*I–L*) from SALS patients. The open arrowheads indicate lipofuscin. There were abundant autophagic vacuoles, e.g., multi-lamellar bodies (arrowheads in *I, K*), autophagosome-like double membrane vesicles (arrows in *K, J*), and autolysosomes (asterisks in *L*) in the motor neurons of SALS patients, but not of the control. Scale bar = 50 μm (*A–C*), 2 μm (*G, H*), or 1μm (*I–L*). Statistical analyses were performed using Student's t test (*p<0.0001) and Pearson's correlation coefficient in *E* and *F*. The error bars are S.E.M.
doi:10.1371/journal.pone.0054511.g001

Moreover, mutations of *DCTN1*, the gene encoding dynactin 1, are linked to familial lower motor neuron disease [14]. Several mutant *DCTN1* models exhibited motor dysfunction and pathological changes related to motor neuron disease [15,16]. As seen in the motor neurons of SALS patients, mutant *DCTN1* mice exhibited a massive accumulation of membrane vesicles, including autophagosomes, in spinal motor neurons [16]. Although these findings suggest that impaired vesicular trafficking might cause the accumulation of vesicles, it remains unclear whether the transport of autophagosomes is actually impaired in the mutant *DCTN1* mice or whether the accumulation of autophagosomes plays a causative role in the pathogenesis of motor neuron degeneration.

The aim of the present study was to clarify the biological link between the quantitative loss of dynactin 1 and the disruption of autophagy. In particular, we examined whether the decreased levels of dynactin 1 induce motor neuron degeneration by

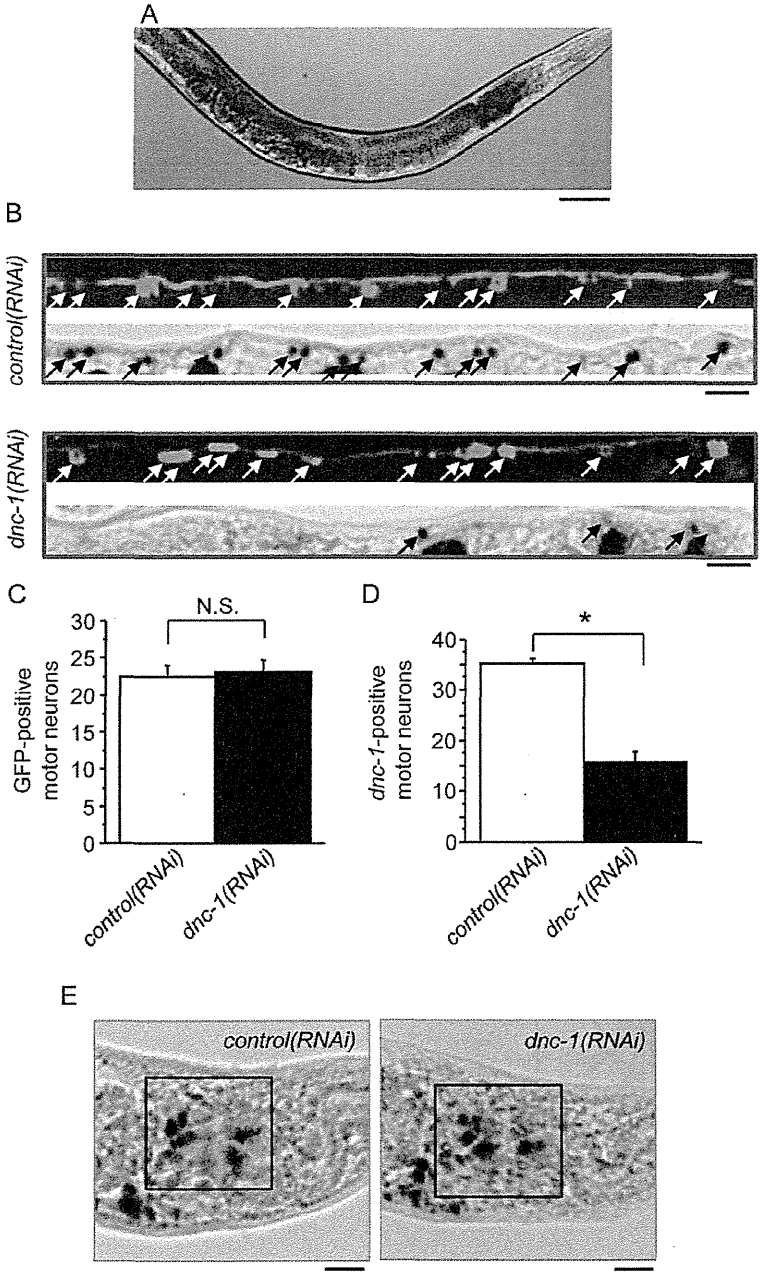

Figure 2. Creation of the motor neuron-specific *dnc-1*-KD *C. elegans* model. (*A*) Fluorescent visualization of ventral cholinergic motor neurons and their neurites in transgenic *C. elegans* worms expressing acr2p::*shRNA*::*gfp*. (*B*) Representative immunohistochemical staining of GFP and *in situ* hybridization against *dnc-1* in ventral cholinergic motor neurons and their neurites in the *control(RNAi)* and *dnc-1(RNAi)* worms. (*C*) The number of GFP-positive motor neurons (white arrows in *B*) was not significantly different between the *control(RNAi)* and *dnc-1(RNAi)* worms (n = 20 animals for each strain). (*D*) Conversely, the number of *dnc-1* mRNA-positive neurons (black arrows in *B*) was remarkably decreased in the *dnc-1(RNAi)* worms (n = 20 animals for each strain). (*E*) Representative images of *in situ* hybridization for *dnc-1* in the head neurons. Scale bars = 100 μm (*A*), 10 μm (*B*), and 20 μm (*E*). Statistical analyses were performed using Student's t test (*$p<0.0001$). The error bars are S.E.M.
doi:10.1371/journal.pone.0054511.g002

hindering the transport of autophagosomes. To this end, we first examined the relationship between the decreased levels of dynactin 1, the accumulation of autophagosomes, and motor neuron degeneration in post-mortem tissues from SALS patients. Next, we created a *Caenorhabditis elegans (C. elegans)* model of the motor neuron-specific knockdown (KD) of *dnc-1*, the *C. elegans* homolog of human *DCTN1*, using small hairpin RNA (shRNA), and investigated whether the depletion of dynactin 1 impairs the transport of autophagosomes and thereby induces motor neuron degeneration. Using this model, we also explored therapeutic strategies targeting the transport of autophagosomes.

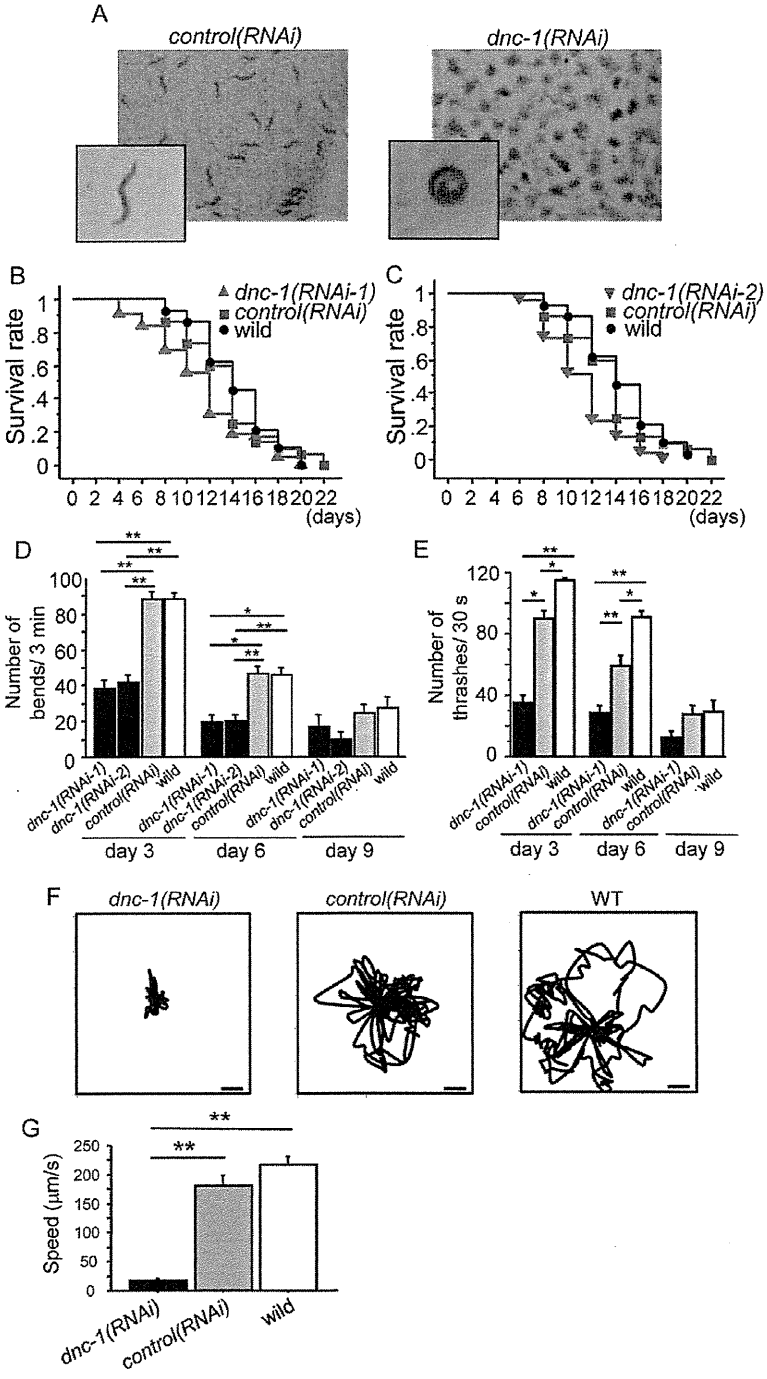

Figure 3. Motor dysfunction in the motor neuron-specific *dnc-1*-KD *C. elegans* model. (*A*) Stereoscopic microscopy showing the phenotypes of the *control(RNAi)* and *dnc-1(RNAi)* worms. (*B, C*) Survival curves of the transgenic worms (*dnc-1(RNAi-1)*, n = 90; *dnc-1(RNAi-2)*, n = 90; *control(RNAi)* n = 90; and wild-type n = 30). The same survival data of the *control(RNAi)*and wild-type worms were used in both graphs. Both *dnc-1(RNAi)* worms with different shRNA sequences (101, 2888) had significantly reduced life spans compared with the *control(RNAi)* worms (101: $p = 0.005$; 2888: $p < 0.0001$; log-rank test). (*D*) The number of body bends associated with forward movement in 3 min. (*E*) The number of thrashing movements in liquid medium in 30 s. (*F, G*) The tracks (*F*) and average speed of the worms (*G*) analyzed by video capture at day 4. Scale bars in *F* = 100 μm. The error bars are S.E.M. (n = 30, 30, 40, and 40 for *dnc-1(RNAi-1)*, *dnc-1(RNAi-2)*, *control(RNAi)*, and wild-type, respectively, in *D*, *E*; and n = 6, 6, and 6 for *dnc-1(RNAi-1)*, *control(RNAi)*, and wild-type, respectively, in *G*). The statistical analyses in *C*, *D*, and *F* were performed by one-way ANOVA followed by the Bonferroni/Dunn post hoc test (*$p < 0.001$ and **$p < 0.0001$).
doi:10.1371/journal.pone.0054511.g003

Materials and Methods

Protocols for the human samples

Ethics Statement. The collection of autopsied human tissues and their use for this study were approved by the Ethics Committee of Nagoya University Graduate School of Medicine, and written informed consent was obtained from the patients' next-of-kin. Experimental procedures involving human subjects were conducted in conformance with the principles expressed in the Declaration of Helsinki.

Immunohistochemistry. Six micrometer-thick sections from paraffin-embedded spinal cord sections from autopsied patients were prepared as described previously [17]: four patients with sporadic ALS (64.5±9.3 years-old; M:F = 2:2) and four disease controls (73.5±5.4 years-old; M:F = 1:3). The four control patients were diagnosed with progressive supranuclear palsy, multiple system atrophy, diffuse lewy body disease, and Parkinon's disease, respectively. The sections were first microwaved for 20 min in 50 mM citrate buffer, pH 6.0, then blocked with TNB blocking buffer (PerkinElmer, Hvidovre, Denmark) in Tris-

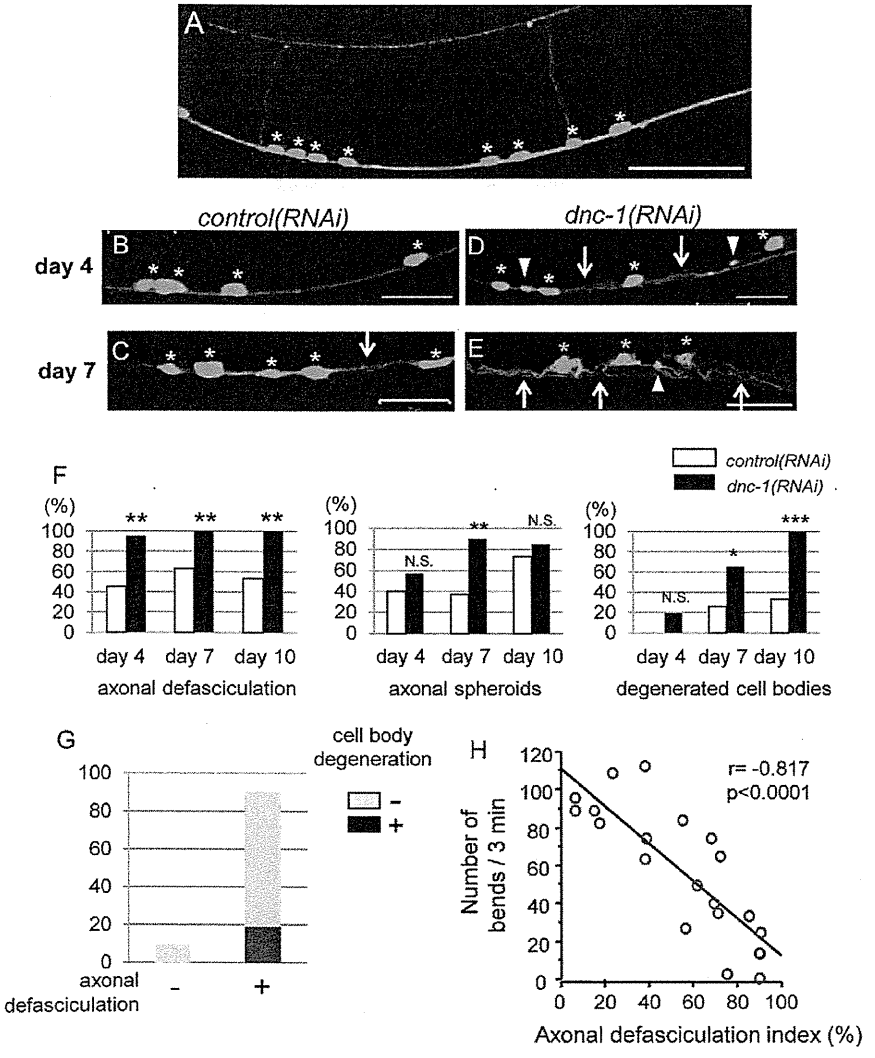

Figure 4. Morphological changes in ventral motor neurons. (*A*) Representative view of fluorescent GFP microscopic images of the ventral nerve cord in a *control(RNAi) C. elegans*. All of the motor neurons (white asterisks) were located in the ventral side of the worm. Axons from the motor neurons project within the ventral nerve cord or toward the dorsal side. (*B–E*) Representative view of the ventral nerve cord in the *control(RNAi)* worms (*B, C*) and *dnc-1(RNAi)* worms (*D, E*). The degenerated axons were defasciculated (arrows in *D, E*) and formed spheroids (arrowheads in *D, E*) in the *dnc-1(RNAi)* worms. Mild defasciculation was observed occasionally in the *control(RNAi)* worms (arrow in *C*). While the cell bodies of the motor neurons were regular and round in *control(RNAi)* and young adult *dnc-1(RNAi)* worms (white asterisks in *B–D*), abnormally shaped cell bodies (yellow asterisks in *E*) were observed only in the worms with severe axonal changes. (*F*) Semi-quantification of the abnormal morphological changes in the *control(RNAi)* and *dnc-1(RNAi)* worms. The percentage of worms with axonal defasciculation, axonal spheroids, or cell body degeneration on days 4, 7, and 10. (*G*) Population of *dnc-1(RNAi)* worms with and without cell body degeneration (black and gray boxes, respectively) on day 4. (*H*) Correlation between the axonal defasciculation index and locomotor function in the *dnc-1(RNAi)* worms. The axonal defasciculation index represents the degree of axonal defasciculation (its details are described in the Materials and Methods). Scale bars = 20 μm. The statistical analysis in *F* was performed using Fisher's exact probability test (*p<0.05, **p<0.001, and ***p<0.0001) and Pearson's correlation coefficient in *H*.
doi:10.1371/journal.pone.0054511.g004

buffered saline (pH 7.5) at room temperature for 30 min and incubated with a monoclonal antibody against LC3 (anti-LC3, 1:40000; Medical & Biological Laboratories, Co., Nagoya, Japan) or dynactin 1 (anti-dynactin 1 H300; 1:2000; Santa Cruz, Santa Cruz, CA, USA) overnight at 4°C. The subsequent procedures were carried out using the EnVision+Kit/HRP (DAB) (DAKO, Glostrup, Denmark) according to the manufacturer's protocol.

Quantitative assessment of immunohistochemistry. To assess LC3 immunoreactivity in spinal motor neurons, we included 4 ALS patients and 4 disease controls, and prepared 5 independent specimens from each subject. We counted about 200 motor neurons in ALS patients and about 400 neurons in control patients. The intensity of immunohistochemistry signals was quantified using a BZ-8000 fluorescent microscope and its software (BZ-Analyzer; Keyence, Osaka, Japan). Signal intensity was expressed as the individual intracellular cytoplasmic signal level (arbitrary absorbance units/mm^2) per motor neuron by subtracting the mean background levels of 3 regions of interest in each section. The ventral spinal horn was defined as the gray matter ventral to the line through the central spinal canal perpendicular to the ventral spinal sulcus. To investigate the correlation between dynactin 1 and LC3 in individual motor neurons we used consecutive transverse spinal cord sections.

***In situ* hybridization.** *In situ* hybridization for human tissue was performed as described previously [13]. We provide the detailed information in Materials and Methods S1.

Electron microscopy. Electron microscopy was performed on samples from 2 sporadic ALS patients (71 years-old male and 62 years-old female) and 2 disease control patients (68 years old male with multiple system atrophy and 60 years-old male with multiple system atrophy). Epoxy resin-embedded specimens of spinal anterior horn were cut into 70-nm ultrathin sections. Ultrathin sections were contrasted by staining with uranyl acetate and lead citrate. Sections were viewed with a JEM-1400EX electron microscope (JEOL, Tokyo, Japan) at 80 kV.

Protocols for *C. elegans*

Ethics statement. All animal experiments were performed in accordance with the National Institute of Health Guide for the Care and Use of Laboratory Animals and were approved by the Nagoya University Animal Experiment Committee.

Culture of *C. elegans*. Standard methods were used to culture *C. elegans* on nematode growth medium (NGM) agar [18]. The animals were maintained at 20°C unless otherwise indicated. We provide the detailed information in Materials and Methods S1.

Constructs and *C. elegans* Strains. To generate transgenic *C. elegans*, plasmid DNA encoding acr2promotor::*shRNA*::*gfp* was injected into the gonads of young adult hermaphrodite N2 worms. We provide the detailed information for the shRNA vector and other co-injected proteins, i.e., SNB-1 and Lgg1, in Materials and Methods S1.

Whole Mount *in situ* Hybridization. Whole mount *in situ* hybridization of worms was performed as described previously [13,19]. We provide the detailed information in Materials and Methods S1.

Phenotypic analysis of *C. elegans*. A lifespan assay was performed as described preciously [20], with some modifications. The Worms were allowed to lay eggs on a dish for 3–6 h to obtain synchronous progeny for the experiment. L4 worms were collected and transferred every 3 days to a fresh plate until the end of their reproductive life. The animals were scored as dead if they did not move when prodded with a platinum pick and did not show pharyngeal pumping.

A body bend assay, liquid thrashing assay, and video capture analysis were performed as locomotion assays. To examine the body bend frequency, exposed worms were transferred onto a fresh NGM plate and scored for the number of body bends

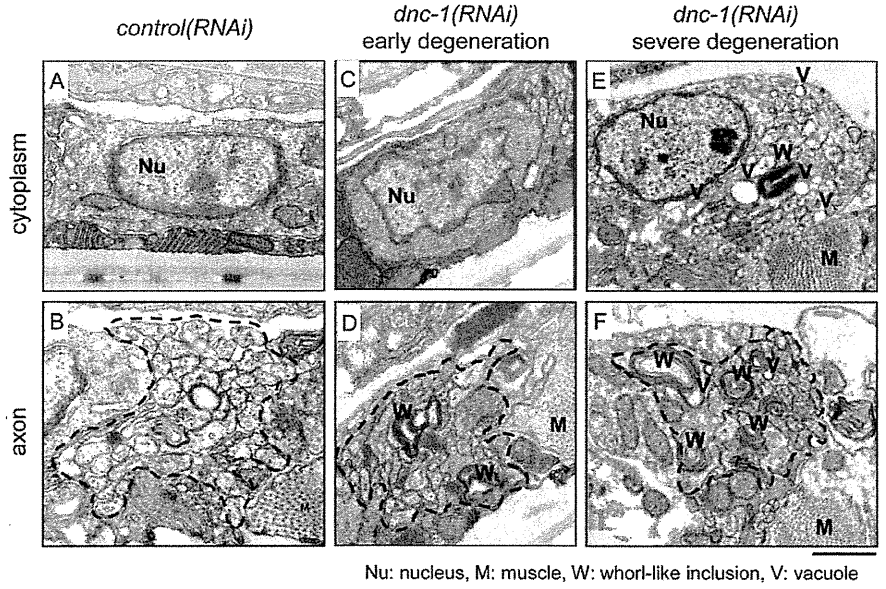

Figure 5. Ultrastructure of degenerating motor neurons. Electron microscopy of transverse sections of ventral motor neurons from the *control(RNAi)* (*A, B*) and *dnc-1(RNAi)* (*C–F*) worms. The dashed lines in *B, D,* and *F* denote the boundaries of the main bundle of axons. Each round-shaped component inside the dashed line is an axon. In the *dnc-1(RNAi)* worms, whorl-like inclusions (W) and vacuoles (V) were observed (*D–F*). In the worms with mild axonal degeneration (*D*), few morphological changes were observed in the cytoplasm (*C*); however, in the later stage with severe axonal degeneration (*F*), the cell bodies were also affected (*E*). Scale bars = 20 μm.
doi:10.1371/journal.pone.0054511.g005

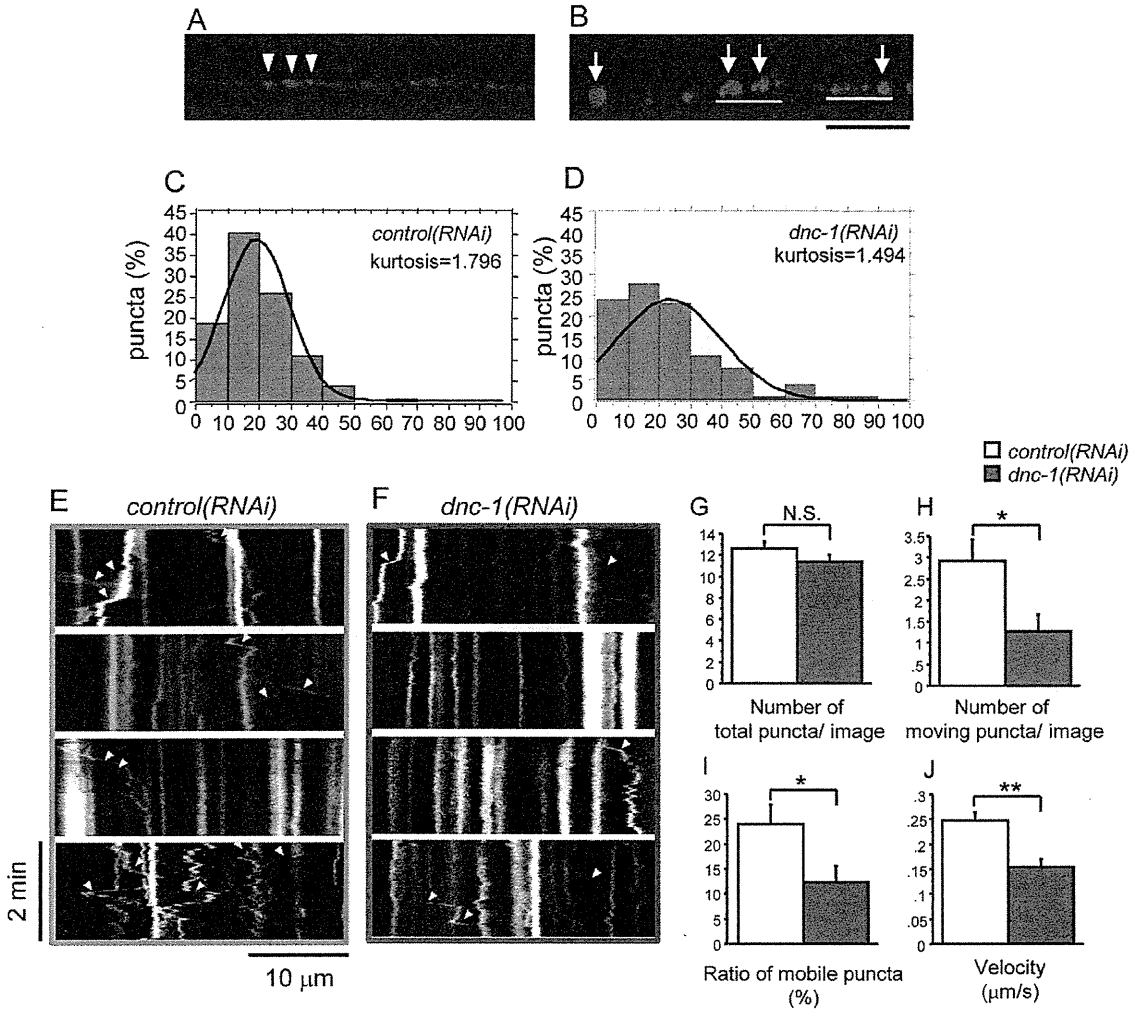

Figure 6. Defective axonal transport of synaptobrevin-1 in *dnc-1(RNAi)* *C. elegans*. (*A, B*) Expression patterns of DsRed-tagged synaptobrevin-1 (SNB-1) in the dorsal nerve cord. In the *control(RNAi)* worms, SNB-1 puncta (arrowheads) are regularly spaced with a uniform shape. In the *dnc-1(RNAi)* worms (B), they are irregularly spaced and abnormally accumulated (white bars) with occasional clumps. (*C, D*) Histograms of the distances between neighboring SNB-1 puncta. The average distance between puncta in the *control(RNAi)* (3.240±1.716 μm, n = 139) and *dnc-1(RNAi)* (3.855±2.764 μm, n = 104) worms was not significantly different (p = 0.996 by Student's t test), but the peak of the control histogram was higher than that of the *dnc-1(RNAi)* histogram, proving that the localization of SNB1 was irregular. (*E, F*) Representative kymographs of SNB-1::DsRed in the ventral nerve cord from the *control(RNAi)* (*E*) and *dnc-1(RNAi)* (*F*) worms derived from time-lapse imaging. Vertical lines represent stationary/docked SNB-1 puncta and oblique lines (labeled with yellow arrowheads) represent the tracks of moving SNB-1 puncta. The slope of this track is an indicator of velocity. (*G*) The number of SNB-1 puncta within a single image of kymograph was not different between the *control(RNAi)* and the *dnc-1(RNAi)* worms. (*H*) The mean velocities of SNB-1 puncta. (*I, J*) The quantitative analysis of mobile puncta. The number of puncta which moved more than 2 μm was counted (*I*). The ratio of moving puncta was calculated by dividing the number of moving puncta by the total number of SNB-1 puncta (*J*). A total of 20 time laps images were analyzed from each strains in *G–J*. Scale bar (black) = 10 μm (*B*). Statistical analyses were performed using Student's t test (*p<0.05, **p<0.001, ***p<0.0001). Error bars are S.E.M.
doi:10.1371/journal.pone.0054511.g006

performed in 3 min. A body bend was defined as a change in the direction of the part of the worm corresponding to the posterior bulb of the pharynx along the y-axis, assuming that the worm was traveling along the x-axis. We also performed a liquid thrashing assay as described previously [21], with some modifications. Briefly, the worms were put on a 6-cm NGM-coated plate with 3 ml of M9 media. The worms were allowed to settle for 30 s, their movements were captured by video for 30 s, and the number of thrashing movements was counted. We also analyzed the speed of movement using a video capture system as described previously [22]. Briefly, fully matured, adult worms were transferred individually to agar plates with no food. The movement of each worm was observed for 5 min and recorded using video equipment (Olympus, Tokyo, Japan) with a sampling rate of 30 frames/s. A computer-controlled microscope stage was automatically moved to center the worms in the visual field using a custom image analysis algorithm within the microscope's software package (MetaMorph; Universal Imaging Corp., West Chester, PA, USA). The midlines of the recorded worms were extracted from each image. All strains were randomized and scored on the same day.